cnrs

F-CRG

cea

LIGNE IF « Interfaces » (BM32)

Diffraction et diffusion des rayons X pour la science des matériaux et les nanosciences

Résumé

Depuis la mise en service des miroirs de ligne et de LaueMAX au début de l'année 2024, l'ensemble des trois instruments est ouvert à la communauté des utilisateurs avec des capacités accrues grâce aux projets MAGNIFIX et DIADEM/ESRF. Au cours de l'année 2025 la ligne a ainsi pleinement accueilli près d'une trentaine d'expériences incluant 45 shifts distribués supplémentaires au nombre convenu annuel. En parallèle, près de 20% du temps de faisceau disponible annuel - en majorité pendant des périodes avec un mode de remplissage dans l'anneau délivrant un faisceau moins intense - a été consacré aux tentatives d'utilisation du détecteur sCMOS dont le dysfonctionnement a perturbé la seconde moitié de l'année (report de 2 expériences), à l'implémentation des workflows de réflectivité sous Ewoks, et notablement aux développements méthodologiques sur les mesures en énergie et résolues en profondeur en microdiffraction Laue. Les progrès significatifs ainsi obtenus sont à la base du succès des campagnes de mesures d'utilisateurs au cours des premiers mois de 2026. Ces performances qui ont été longtemps en point de mire ont été atteintes aussi grâce à la rapidité et la précision des images collectées par le nouveau détecteur EIGER 4M CdTe. Au printemps 2026, la ligne a été auditée par un comité international conformément au programme d'évaluation quinquennal des lignes de lumière à l'ESRF. Les conclusions du comité rapportent l'excellent positionnement de la ligne sur les mesures *operando, in situ*, multimodale et multiéchelle pour la science des matériaux et les nanosciences. Des recommandations sont formulées pour améliorer le service aux utilisateurs et augmenter la production scientifique quant aux futurs développements nécessaires envisagés, notamment logiciels, le fonctionnement et la valorisation d'instruments à haut potentiel scientifique.

Les ressources humaines nécessaires supplémentaires souhaitées pour un meilleur fonctionnement de la ligne dans les futures années sont décrites plus en détails dans la dernière section de ce rapport (§3). Elles s'inscrivent dans les trois axes essentiels de progression par des positions au caractère :

- scientifique sur INS2 afin que la communauté profite pleinement des atouts de l'instrument,
- technique pour la préparation et l'accueil des expériences *in situ* et *operando,*
- informatique pour assister les développements logiciels pour le traitement de données et prendre le train des solutions à venir basées sur l'IA.

Statistiques d'utilisation de la ligne IF

Nous donnons dans cette partie les éléments chiffrés relatifs à l'exploitation du temps de faisceau et à l'origine des utilisateurs. Ces chiffres et leur évolution seront mis en perspective grâce aux données synthétisées à l'occasion du récent audit international BeamLine Review Panel (BLRP) organisé par l'ESRF pour l'évaluation des lignes de lumières (publiques et CRG).

1.1. Allocation du temps de faisceau

utilisation faisceau	total	INS2	GMT	Laue	
	682	178	54	450	
utilisation faisceau	total	utilisateurs temps ESRF	utilisateurs temps CRG	BLC, buffer, test faisabilité	IHR (temps de recherche propre)
	682	183	285	120	86

Pour la période d'exploitation du faisceau pendant l'année civile 2025, la répartition des shifts (8 heures) est donnée dans le tableau ci-dessous selon deux répartitions, soit par instruments soit par type d'utilisation :

- Plus des 2/3 du temps de faisceau délivré par l'ESRF (total 682 shifts) a été employé pour le service aux utilisateurs sur les trois instruments (INS2, GMT, Laue) correspondant à près de 30 équipes d'utilisateurs et une durée moyenne de près de 15 shifts par expérience. Au cours de l'année civile 2025, l'équivalent de plus de 3 expériences supplémentaires de services aux utilisateurs ont été programmés (2 promotions et des prolongations) sur contingent ESRF.
- Près de 20 % pour des tests de faisabilité, du temps de buffer (pour des transitions entre expériences et des compléments de temps d'expériences pour simplifier le calendrier des alternances entre instruments), du commissioning (BLC) de nouveaux équipements et parfaire des méthodologies (principalement Mesure en résolue en énergie et en profondeur sur LaueMAX, MAGNIFIX) et implémenter des workflows sous ewoks pour la réflectivité (GMT, DIADEM)
- Moins de 15 % pour du temps de recherche propre (IHR) principalement relié aux scientifiques, post-docs et étudiants en thèse dans le groupe NRX de l'IRIG/MEM.

L'année civile 2025 est donc marquée par un service plus que complet aux utilisateurs et un fort emploi du temps restant pour les développements instrumentaux dans le cadre de MAGNIFIX et DIADEM.

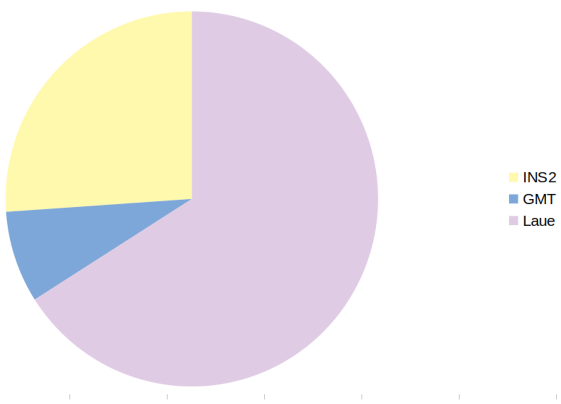

Figure IF-1: répartition du temps de faisceau (682 shifts) en 2025 sur IF par instrument. Une très grande majorité du temps a été passé sur LaueMAX pour les utilisateurs et parfaire les mesures menées et les développements méthodologiques (Diamant et DAXM).

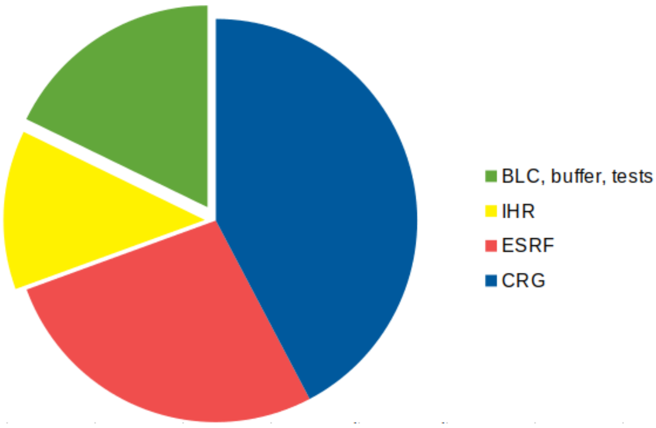

Figure IF-2: répartition des 682 shifts de faisceau par utilisation en 2025: ESRF (temps international), CRG (temps français), BLC (beamline commissionning), buffer (temps tampon entre expériences), test de faisabilité, IHR In-house Research.

1.2. Statistiques d'attribution 2025

Nous avons pu programmer du temps de faisceau correspondant aux propositions d'expérience soumis lors des deux appels de 2025 sur les deux comités ESRF et CRG (SOLEIL).

Appel Fév. Mars 2025	shifts demandés	shifts à distribuer*	alloués	pression (shifts demandés/shifts à distribuer)
CRG (AP 36)	105	90	120	1.2
ESRF	249	75	90	3.3
Appel Sept. 2025				
CRG (AP 37)	268	140	153	1.9
ESRF	158	67	70	2.4

Résultats en shifts et nombre d'expériences entre parenthèses des deux appels à projets en 2025 pour du temps ESRF et CRG (SOLEIL). Contractuellement, la ligne doit distribuer près de 70 shifts par semestre aux comités ESRF et le double, 140 shifts, aux comités CRG (SOLEIL). (*) Prévision du montant des shifts à distribuer au moment de l'appel. Au moment de la planification des expériences, la ligne, la plupart du temps, distribue plus de shifts par le jeu des promotions et de temps additionnels pour augmenter les chances de réussites des mesures.

Au moment de l'appel à projets sur les deux contingents, nous adaptons la quantité de temps minimale à distribuer sur le temps français. Cela donne un levier permettant d'équilibrer éventuellement les expériences programmées sur INS2 et LaueMAX. Depuis peu, le premier des deux appels pour obtenir du temps de faisceau pour la communauté française est souvent négligé avec une demande plus faible (temps français pour les appels de février et ESRF pour ceux de septembre). Le second appel à projets quinze jours plus tard bénéficie d'un nombre de demandes supérieur grâce à une campagne de communication intense auprès des anciens utilisateurs et ceux rencontrés en conférence ou dans des séminaires. Ainsi certaines équipes ne soumettent que sur le temps ESRF. A ce titre, les appels du début de l'année 2025 ont été particulièrement compliqués.

A l'issue des résultats sur les temps CRG et ESRF, nous procédons ainsi fréquemment à la promotion des équipes françaises sur des listes de réserve ESRF. La pression est donc souvent faible sur le temps CRG et très satisfaisante sur le temps ESRF. A l'avenir, nous comptons anticiper et mieux préparer les laboratoires français des 2 échéances annuelles.

Données sur les six dernières années (BLRP)

Nous donnons dans cette partie des éléments chiffrés relatifs à l'utilisation du temps de faisceau pour la période civile 2020-2025 inclus.

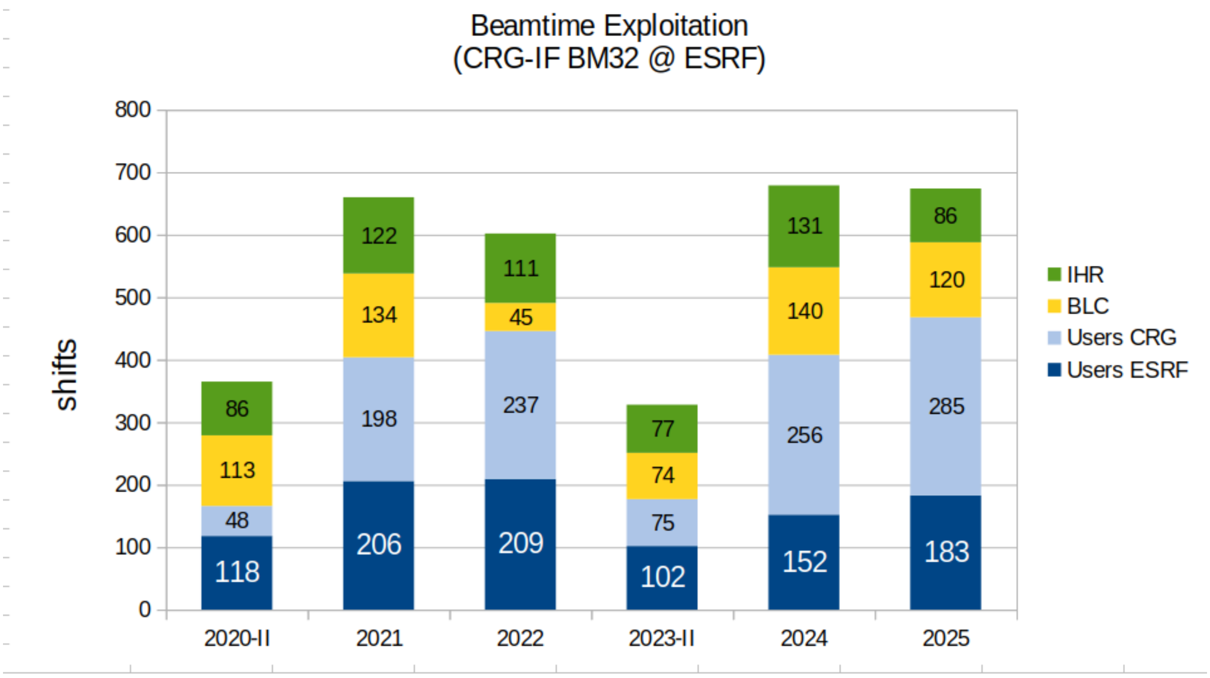

Figure IF-3 : exploitation du temps de faisceau par la ligne de lumière IF pendant la période 2020-2025 et sa répartition par utilisation, pour les propositions sélectionnées par les comités ESRF et CRG : mise en service d'instruments, de détecteur, et la mise en œuvre de méthodes expérimentales (BLC BeamLine Commissionning), temps de recherche propre (IHR In-House Research) et temps d'expérience utilisateurs CRG ou ESRF. Ces données sont construites à partir des shifts effectivement réalisés et regroupées par année civile (du 1er janvier – sauf du 1er septembre en 2020 et 2023 – au 31 décembre).

Depuis l'année dernière (2025) le volume de temps pour le service aux utilisateurs est revenu au niveau (et même légèrement supérieur) des 420 shifts annuels (140 ESRF, 280 CRG) (cf figure IF-3). Précédemment, l'accueil avait été un peu réduit en raison de la nécessité à consacrer du temps BLC et IHR pour la conception et la réalisation des nouveaux instruments et méthodes. On rappelle ci-dessous les principaux temps non consacrés à l'accueil des utilisateurs : du temps IHR et du temps BLC principalement dédié à des mises en place et tests pour LaueMAX, la ligne de lumière et le PEPR DIADEM : redémarrage de la ligne après réalignement, tests de stabilité, développement des méthodes diamant (rainbow) et DAXM, la mise en œuvre du four QMAX, la résolution des problèmes liés au détecteur sCMOS, implémentation du cristal analyseur (INS2), l'intégration d'ewoks (GMT). Une partie du faisceau sert aussi à des temps tampon entre expériences ou pré-alignement, des tests de faisabilité, des travaux pratiques pour les étudiants HERCULES et Master 2, etc…

Sur la figure IF-4, sont représentés les volumes de shifts demandés et délivrés. Ces données concernent uniquement les comités ESRF. On peut noter la pression entre 2 et 5. Cette pression a beaucoup fluctué durant les dernières années indiquant des signes de faiblesse de l'attractivité de la ligne, très souvent indiqués dans les rapports d'activité antérieurs. Nous constatons que l'attractivité est encore trop dépendante de la mobilisation du personnel à valoriser les progrès réalisés et la profonde évolution des équipements altère à la fois le service aux utilisateurs et ainsi que la lisibilité nécessaire pour se projeter dans des projets sur notre ligne.

Sur le temps CRG, non représenté ici, la pression est deux fois moindre (1 – 2.5), certaines équipes françaises ne soumettant que sur du temps ESRF, rendant quelquefois l'appel critique au point de devoir diminuer au moment de l'appel à projet la quantité de temps à distribuer, puis dans un second temps promouvoir depuis la liste de réserve ESRF des propositions d'expériences françaises.

Nous pensons que l'attractivité est de nouveau importante avec plus de 350 shifts demandés sur le temps ESRF au dernier appel, grâce aux efforts du personnel à communiquer en conférences et partager avec la communauté des fortes nouvelles potentialités des instruments et des équipes.

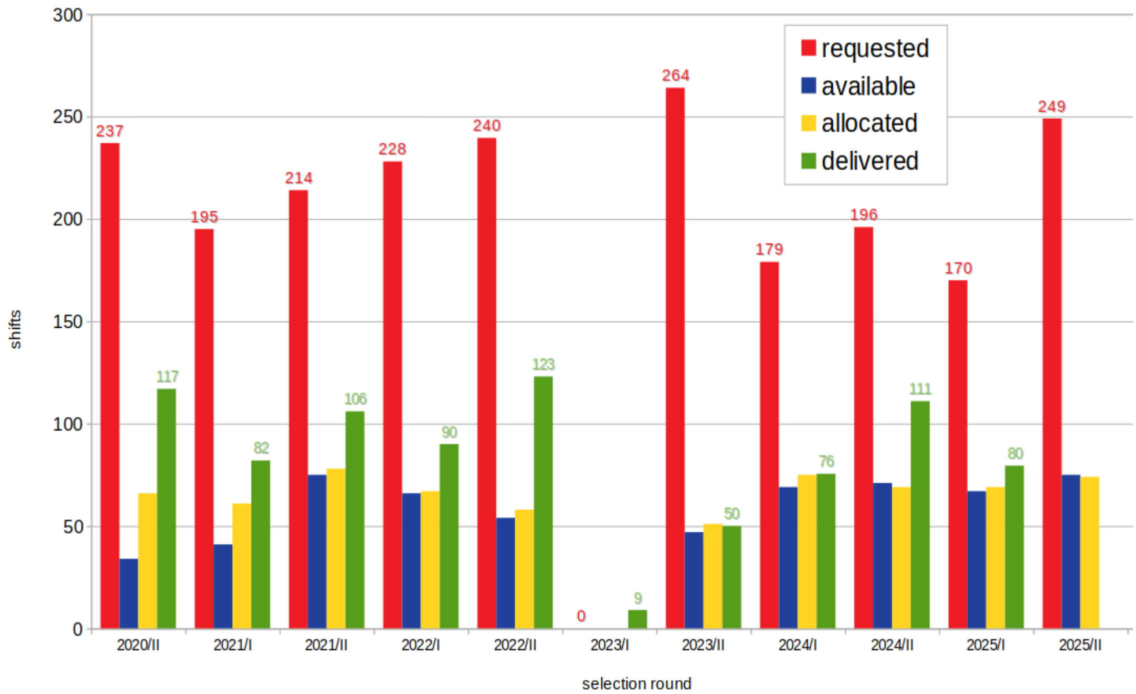

Figure IF-4: distribution lors des 10 derniers appels à projets sur le temps de faisceau ESRF depuis la reprise en septembre 2020 (nouvelle source ESRF EBS) sur CRG-IF BM32 par catégorie: Requested: quantité de shifts demandés; Available: quantité de shifts disponibles (par contrat CRG-ESRF ~ 70 shifts) au moment de l'appel; Allocated: quantité de shifts alloués au moment de la programmation (en tenant compte des résultats des comités CRG); Delivered: quantité de shifts effectivement délivrés et réalisés après promotion d'expériences et de prolongation. Note: en 2023, la ligne était fermée pendant un semestre pour le démantèlement et la reconstruction de la cabane EH1 pour LaueMAX.

Thématiques des utilisateurs

Les comités de programmes sélectionnant les propositions d'expériences sont inchangés. Ils correspondent à nos domaines scientifiques majeurs : science des matériaux et nanosciences par des mesures de diffraction diffusion des rayons X. Les principaux comités de programme SOLEIL sont PRC3 ('Propriétés de la matière et des matériaux : Structure, Organisation, Caractérisation, Elaboration') et PRC4 ('Propriétés de la matière et des matériaux : Structure, Organisation, Caractérisation, Elaboration'), tandis que les propositions d'expériences ESRF parmi les 12 disciplines scientifiques sont dans les domaines MA ('Applied Material Science'), HC ('Hard Condensed Matter Science') et SC ('Soft Condensed Matter Science').

Origine des utilisateurs

Les laboratoires français concernés par le temps faisceau en 2025 proviennent équitablement du CEA dont une partie de laboratoires mixtes CEA-CNRS (SyMMES et ICSM) et du CNRS. On peut ajouter que le temps IHR est majoritairement utilisé par des agents de laboratoire du CEA-Grenoble/IRIG (MEM et SyMMES) mais qu'il n'apparaît dans le présent décompte. Un tiers des utilisateurs proviennent d'équipes internationales ce qui correspond approximativement à ce qu'on attend de la répartition contractuelle CRG-ESRF de 2/3 et 1/3. A noter, le caractère approximatif des chiffres voire déformant lorsqu'une équipe de 5 à 6 personnes comparé à des équipes de 2 seulement vient pour une durée d'expérience semblable.

Figure IF-5 : répartition du temps officiel distribué aux utilisateurs par laboratoire d'origine en 2025 (temps d'expérience X proposeurs présents au moment de l'expérience déclarés sur le form A (en shift.utilisateur). Ce calcul favorise les équipes venant en nombre sur la ligne au détriment d'utilisateurs venant pratiquement seul.

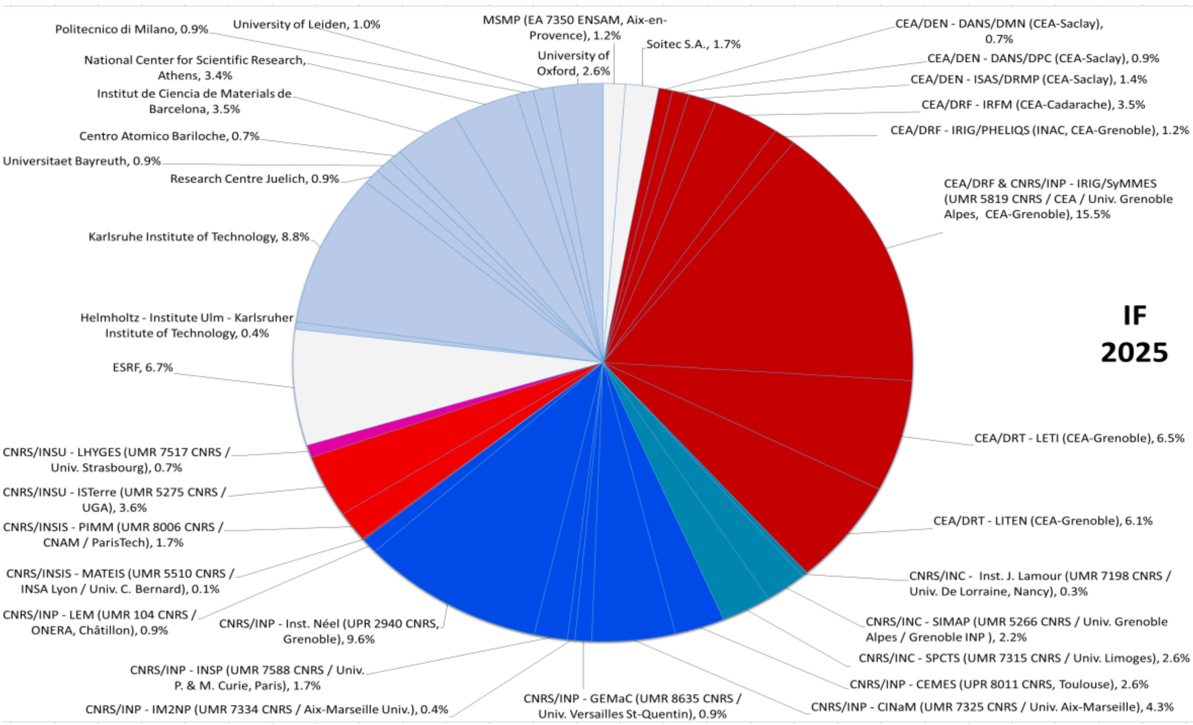

Les proportions d'utilisateurs CEA, CNRS, ou de laboratoires étrangers restent assez constantes. La distribution instantanée en 2025 (figure IF-5) est d'ailleurs très similaire à celle effectuées sur les six dernières années (figure IF-6). On pourra noter qu'en raison des promotions que nous effectuons depuis la liste de réserve ESRF évoquées plus haut parmi les 1627 shifts délivrés à la communauté française, 861 proviennent du temps de faisceau ESRF, indiquant une forte présence des équipes sélectionnées sur la ligne IF sur du temps ESRF.

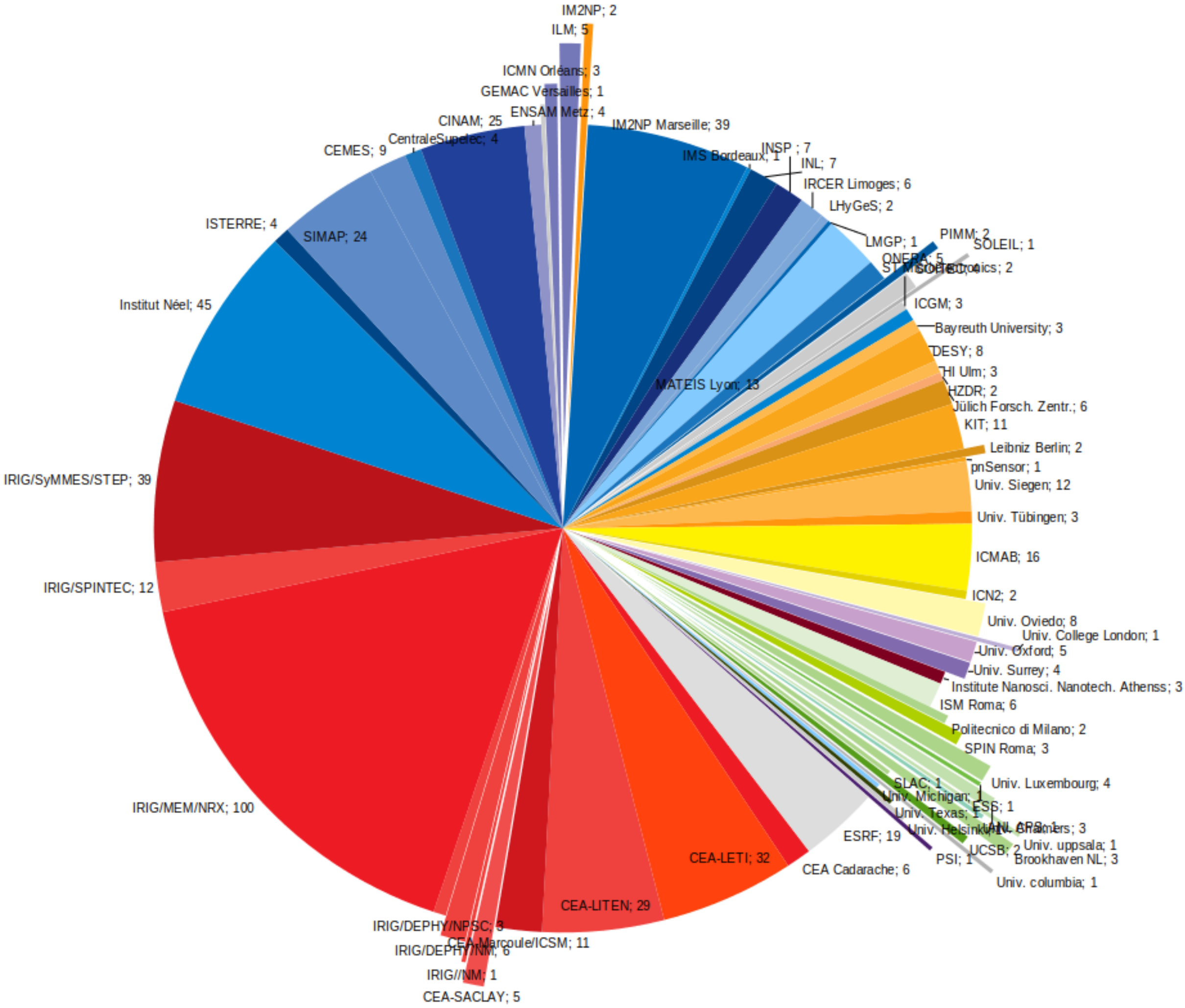

Figure IF-6 : Distribution des utilisateurs (par laboratoire) déclarés sur le form A des expériences effectuées sur la ligne de lumière (2020-2025) temps ESRF et CRG. (en nombre d'utilisateurs).

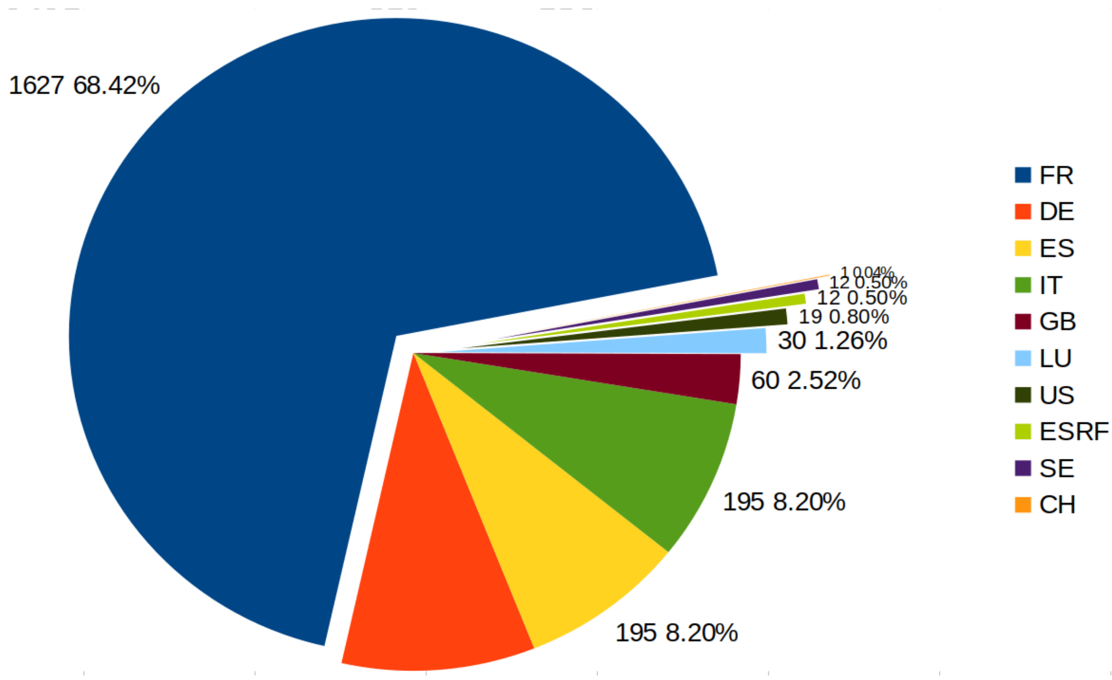

Figure IF-7 : Quantité de shifts délivrée (de 2020 à 2025) sur BM32 (temps de faisceau ESRF et CRG) par pays *d'origine du porteur principal de la proposition. Le premier chiffre indique le nombre de shits, le second le ratio par rapport au total de 2378 (en %). Le code pays correspond à la localisation du laboratoire du porteur principal : FR (France), DE (Allemagne), ES (Espagne), IT (Italie), GB (Royaume-Uni), LU (Luxembourg), US (États-Unis), SE (Suède), CH (Suisse).*

1.3. Allocations prévues pour 2026

Pour l'appel à projet de février-mars 2026, nous avons décidé, compte tenu du niveau des demandes en progression mais un peu faible sur les comités français (174 shifts demandés/ 140 shifts normalement distribués), de distribuer 125 shifts sélectionnés par les comités SOLEIL, de manière à ne pas accepter mécaniquement des propositions d'expériences parmi les moins bien classées d'un point de vue scientifique. Nous avons aussi besoin d'être en mesure de répartir de manière équilibrée les charges d'accueil sur les trois instruments et en fonction des résultats sur les comités ESRF. Dans la mesure du possible, nous promouvons des expériences d'équipes françaises issues des listes complémentaires ESRF.

2. Développements méthodologiques et instrumentaux de la ligne IF

L'année 2025 correspond à l'achèvement du projet MAGNIFIX (incluant la mise en service du détecteur EIGER en janvier 2026) et la poursuite des développements des plateformes ciblées à l'ESRF dans le cadre du PEPR/DIADEM. Les paragraphes suivants en anglais sont une sélection des développements décrits dans le BLRP 2026 pour lesquels des progrès notables ont été obtenus à partir de 2025.

During the 5 last years, the beamline staff was extremely committed to the achievement of the MAGNIFIX project (2021-2026). We mainly refurbished the essential optics elements to benefit from the reduced X-ray source size provided by the EBS upgrade programme and we moved the Laue microdiffraction instrument towards high throughput data acquisition and analysis and towards more routine measurements of new structural parameters, with complementary depth-resolved and energy measurements.

In parallel to these major works, the beamline pursued the improvement of the techniques and methods by means of hardware and software development. Among other developments regarding the control of sample environment setup (furnaces, electrodes, etc.) we would like to underline the implementation of crystal analyser on INS2, our effort to limit the KB mirrors performance degradation with time and the integration of the fast and high capacity samples changer on GMT.

Software-related issues were identified as the main bottlenecks of the beamline productivity very early. Our first priority was the full integration of BLISS, the migration of our acquisition macros and the programming of new ones - that were impossible to implement with *SPEC* in the past. Concerning data analysis, we have kept developing home-made data analysis softwares for Laue diffraction, started using *Binoculars* for handling reciprocal space map data, and also initiated X-ray reflectivity inversion pipeline. At the same time, to fit the needs of the communities for X-ray scattering we managed to migrate (if needed) from 0D to 2D detectors for WAXS measurements over a large angular range on GMT. Moreover, we determined the best experimental conditions to obtain reliable structural information in sensitive electrochemical systems. Finally, we gained expertise in the handling of hyperspectral data by using Machine Learning factorisation algorithms.

LaueMAX

To generate the pink microbeam, we use a classical Kirkpatrick–Baez (hereafter KB) microfocusing system consisting of two elliptically bent, mutually perpendicular silicon mirrors. The KB mirrors are iridium-coated and operate at a fixed incidence angle of 2.8 mrad, providing a cutoff energy of 27 keV. The first KB mirror is 290 mm long, and the second is 140 mm long. The KB system demagnifies the ESRF source located 45000 mm upstream. The demagnification factor is defined as the ratio between the object distance and the image distance. To maximize demagnification, the KB optics are positioned as far as possible from the source and as close as possible to the sample, resulting in demagnification factors of 355/45000 in the vertical plane and 120/45000 in the horizontal plane.

To minimize beam spot broadening caused either by mirror polishing slope errors or by imperfect mirror bending, special care was taken with the optical quality. The slope errors of the bendable beamline mirrors M1 and M2 manufactured by Winlight System (France), are below 0.15 µrad over their central 200 mm, while the KB mirrors manufactured by JTEC company (Japan) exhibit slope errors below 0.1 µrad over their full length.

Since the instrument must be retracted when the beam is used in the GMT or INS hutches, it was designed to allow for simple and rapid removal. The instrument consists of a stack of three granite blocks resting on a granite base bonded to the floor. The high-precision repositioning system enables very fast realignment when beam operation resumes. The stacking of the two upper granite blocks allows easy vertical adjustment, enabling selection of the cutoff energy by tuning the mirror angles in the optical hutch. To optimize the beam size while limiting aberrations introduced by each optical element, it is also possible to use only the M1 mirror in the optical hutch. In this configuration, the beam becomes upward deflected toward the Laue MAX instrument; the instrument's vertical adjustment capability then accommodates this geometry.

The horizontality of the uppermost granite block, which supports the focusing optics and the sample, is actively stabilized with a piezo actuator using feedback from an inclinometer. This system compensates for slow drifts of the concrete floor. The sample, positioned at 40° relative to the incident beam, is mounted on a motorized XYZ translation stage with a resolution of 20 nm. A piezoelectric cube can be added to achieve a positioning resolution of 2 nm for light-weight samples.

A retractable microscope allows beam alignment on a thin single-crystal YAG screen and identification of regions of interest on the samples. On the side, mounted on an articulated arm, a silicon drift detector (SDD) enables fluorescence mapping as well as beam size measurements using a knife-edge scanning method.

Above the sample, since January 2026, a CdTe Eiger 4M pixel detector collects Laue diffraction patterns. It can be positioned at angles ranging from 0° to 88° relative to the incident beam and at sample-to-detector distances varying from 70 mm to 380 mm. This flexibility allows maximizing either the number of collected diffraction peaks or the angular resolution on a single spot.

The overall instrument was designed at CNRS-SERAS under the supervision of the beamline team. The assembly and testing of the instrument were carried out by the beamline staff.

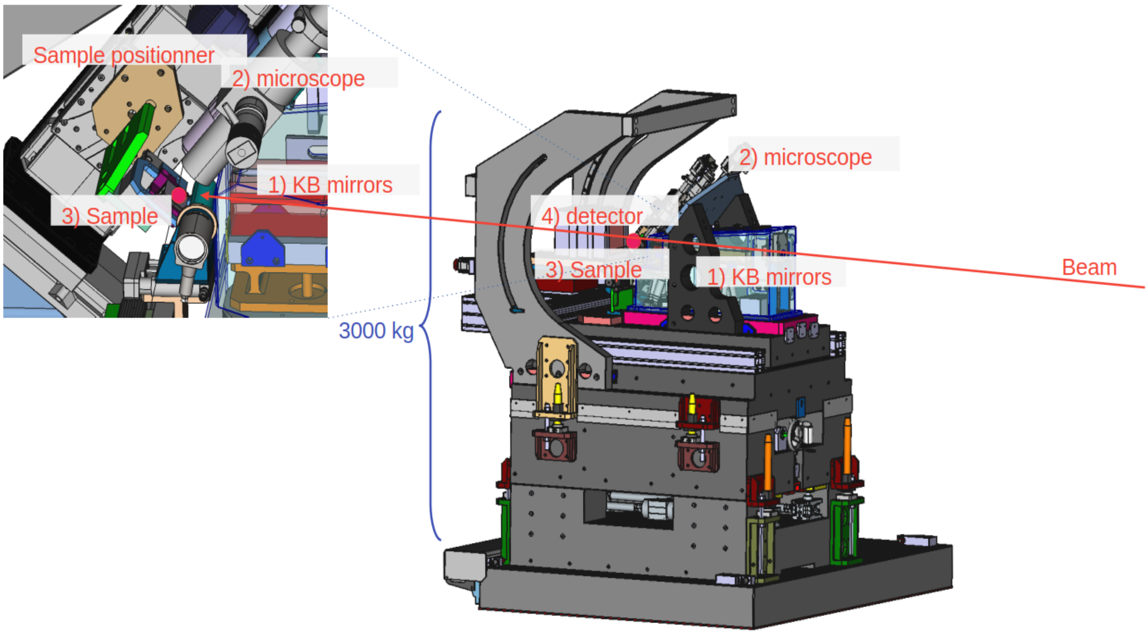

Figure IF-8: New LaueMAX instrument, designed by BM32-IF beamline and CNRS-SERAS and funded by MAGNIFIX project.

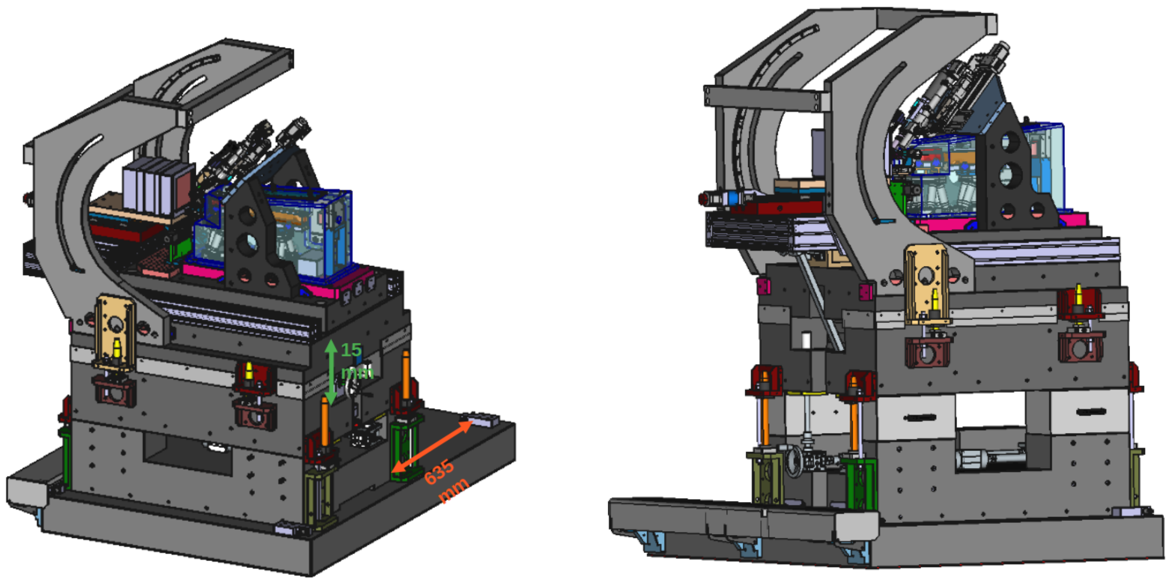

Figure IF-9: The LaueMAX instrument resting on granite blocks with elevation and tilt adjustment systems that allow it to operate at two different heights (corresponding to favoring flux or extremely small beam size) and to correct slow angle variations of thermal origin, coming from the ground or the ESRF beam, respectively. The detector (shown here lying flat in transmission mode) can be positioned around the sample at varying distances. The instrument can be retracted to make room for a transfer tube for experiments conducted on GMT (EH2) or INS2 (EH3).

To install this new instrument, a new experimental hutch was constructed, replacing the former EH1 hutch originally built at the inception of the beamline. The new hutch was designed to position the LaueMAX instrument as far as possible from the source, without requiring modifications to the control room. The sample is located 45 m from the source, while the end of the second focusing mirror is positioned only 4.5 cm from the sample. The hutch was extended upstream to the maximum possible extent to allow for the potential future installation of a toroidal mirror.

The demolition of the former EH1 hutch and the construction of the new enclosure took place from mid-March to early September 2023. Installation of the instrument base was carried out during the winter shutdown in early 2024, followed in January by the transfer of components reused from the previous setup. Optical performance measurements of LaueMAX were conducted at the end of March 2024, confirming a tenfold increase in flux compared to the previous configuration. After a short alignment phase, a beam size of 200 nm × 300 nm (H × V) was achieved at the sample position.

LaueMAX renewed instrumentation was opened to the user community in April 2024. Subsequent commissioning periods further improved the beam size and optimized the alignment procedures. All alignment scans for beam size optimization are now performed continuously ("fscan" for fly or fast scan) without dead time related to stopping the translation motor, using *BLISS* (duration ~10 seconds).

Since January 2026, the new purchased detector EIGER 4M CdTe allows as well flyscan for Laue pattern measurement of scientific interest.

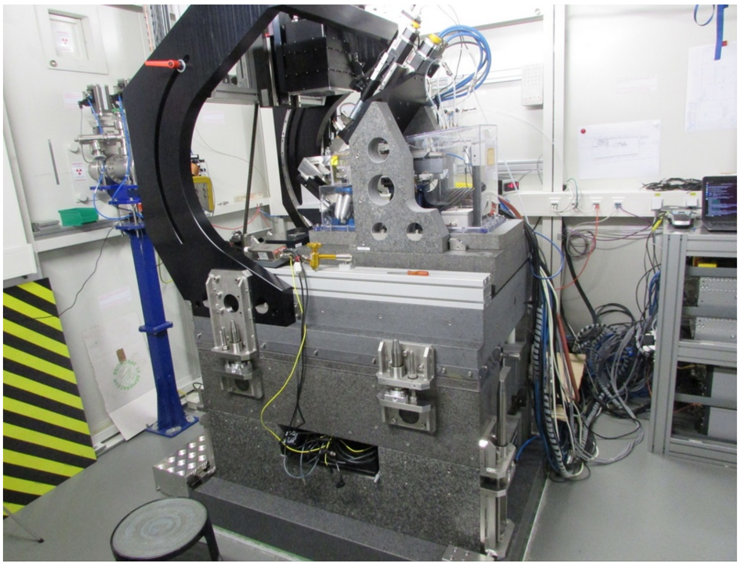

Figure IF-10: The new Laue microdiffraction X-ray microscopy station, LaueMAX, located in the new dedicated hutch EH1 on the BM32 beamline. It is mounted on granite blocks and can be retracted while keeping all equipment connected, making way for a transfer tube when experiments are conducted on GMT and INS2. This design allows the instrument to restart in just 1 to 2 hours.

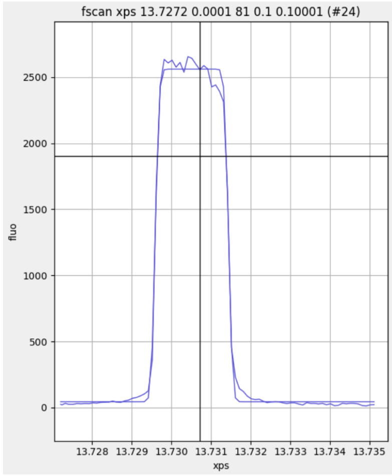

Figure IF-11: Variation in the fluorescence signal intensity (black curve) during a horizontal scan of a 2 µm wide (0.25 µm thick) copper pattern, used to determine the beam size in the horizontal direction (here, 200 nm, as fitted by a model with the blue profile).

Measuring Laue spot energies

The retrieval of Laue spot energies is performed by using the so-called “Rainbow” method with the recently purchased 2D fast pixel hybrid detector, after the evaluation of a too limited capacity of energy-resolved solid-state detector. The “Rainbow” method consists in removing controlled wavelengths from the incident beam using a rotating diamond single crystal filter. Spot energies provide *dspacing* (interatomic lattice planes distance = dHKL’s distances) and unit cell volume, to determine the full set of lattice parameters or equivalently the full strain tensor, which is important to assess the full stress tensor. To reach the 10-4 angular resolution, precise experimental determination of scattering angles by means of 2D detector is crucial. The measurement of a Laue spot energy is based on the determination of the local minimum in the intensity profile (hereafter called ‘dip’).

With the switch to *BLISS* acquisition software in 2022, it became possible to set up a “multi-branch” *Edia* diamond energy pseudomotor. Simple macros using the pseudomotor then automatized successive cutting of the same spot energy with several diamond branches, over a 360° angular range. This allowed using the sample itself to cross-check the calibration of diamond geometry, for improved accuracy.

In February 2024, the insufficiently accurate Newport RVS80PP diamond rotation stage was replaced by a Huber 409 optically-encoded stage, offering 0.001° absolute accuracy. The Rainbow setup is now available on a retractable rail, upstream of the LaueMAX setup. It features vertical and horizontal linear stages, the ImageStar9000 camera for collecting diamond Laue patterns for pre-alignment, and the rotation stage.

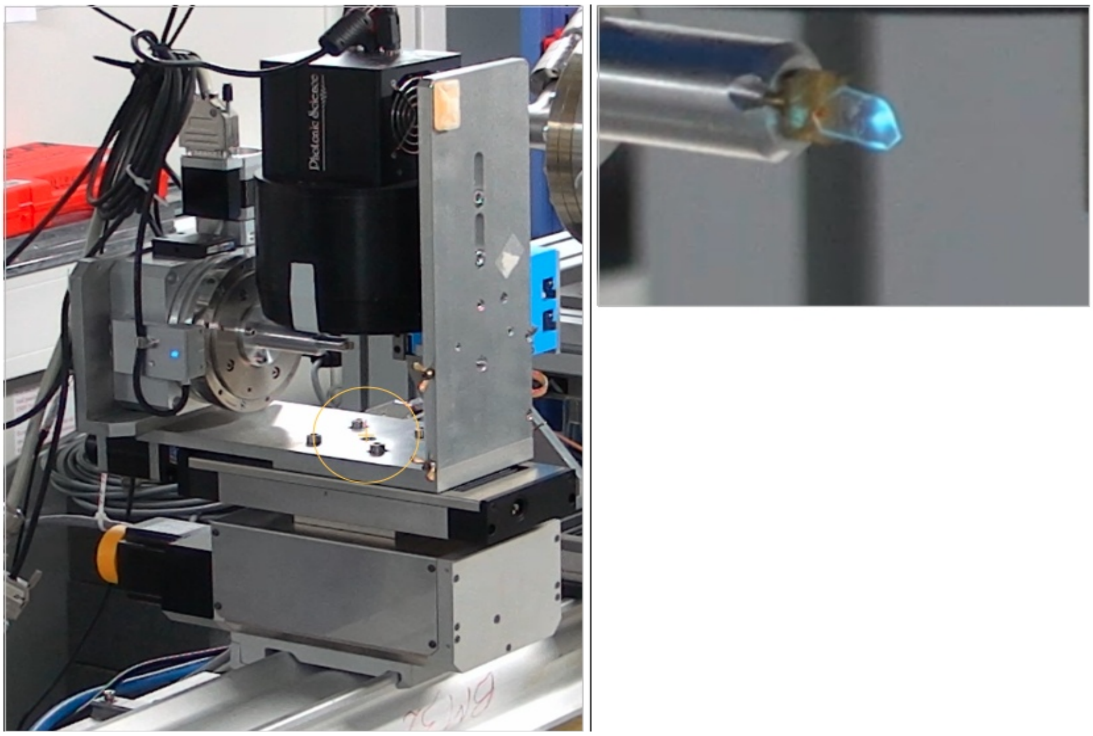

Figure IF-12: Setup for the diamond filter (so-called rainbow method) acting like a parallel monochromators (for the transmitted beam illuminating the specimen of interest downstream) by attenuating photons flux for a set of photons energies that can be tuned (and calibrated) as a function of a single angle thf. The setup enables the experimental determination of the photons energies of one or several Laue spots of a Laue pattern.

Gaining expertise in correcting grid-distortions of the 2D detectors was found necessary. "Ten pixels for the price of one" are needed for accurate conversion of x,y of spots into 2theta angles. Quad sCMOS Photonics Science detector was found to give 0.07° error on 2theta values after remapping with manufacturer's software. Rainbow results had to be used to decide on the (arbitrary) non-distorted "reference" grid unit cell used for defining distortions, when analysing grid-shadow images (grid lent by ID15, PyFAI notebooks from BM02). By contrast, 2theta values were already accurate to 0.005° with the Eiger 4M CdTe detector (without further correction). Distortion-correction on Eiger images still helps improve accuracy on strain : pixel deviation when fitting unit cell shape and orientation, to match x,y spots positions in the Laue pattern, decreases from 0.42 to 0.24 pixel.

The script for fitting diamond rotation geometry ("calibdia.py"), which uses the thf_dip values of 16 or 24 dips, from 8 branches times 2 or 3 spots of Germanium, now includes simultaneous refining of Ge orientation with respect to incident beam. This was used to check the quality of grid-distortion corrections.

Python scripts are also available for 1) post-recalculation of rois around all spots (indexed or not) from a several series of Laue patterns collected during thf-scans, 2) for replotting all rois automatically organized on a series of plots and 3) in the case of indexed spots, for adding labelled vertical markers at theoretical dip positions, and sorting curves according to energy. This latter plot helps lift dip indexation ambiguities, by easy eye-tracing of abacus branches.

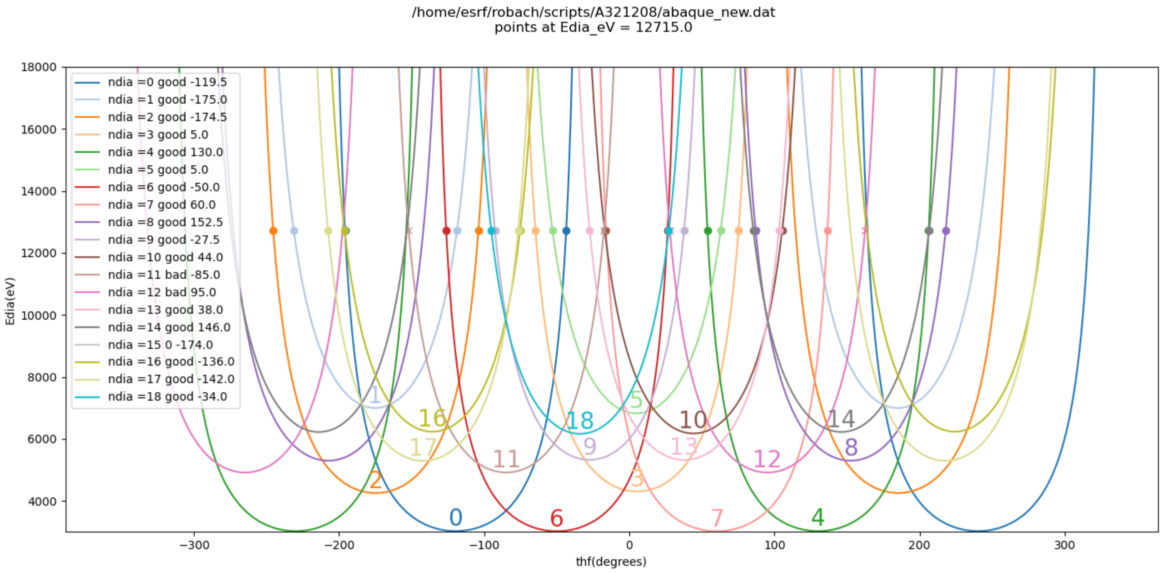

Figure IF-13: energy vs angle multi-branch abacus of the rotating diamond filter. Each ndia corresponds to a single diamond (HKL) diffraction branch. Two branches of type "m" and "p" per ndia. Only {111} and {220} branches are shown. The pseudomotor covers a single branch. (nickname : "Tarzan")

BLISS macros are now available for collecting and analyzing energy scan data at several sample spots, each with several diamond branches, based on the LaueTools-generated ".fit" results text file of an already-indexed grain. Continuous scans, with roi counters around spots, were set up in February 2026. Thanks to continuous scans and increased dynamic range, previously unmeasurable dips could be accurately measured, by scan repetition and roi-to-rois normalization, on the difficult case of a dip occurring on an harmonic of the fundamental energy, on a submicron grain of a monoclinic phase of AlFe. Another difficult case of diffuse spots of nitrided Ni5%Ti on top of strong Ni fluorescence could also be addressed. Here the Eiger threshold was increased to cut Ni fluorescence and increase signal-to-background ratio. For such diffuse spots, it is still possible to obtain sharp dips by dividing the spot into "same 2theta" slices and plotting slice intensities versus dHKL instead of Edia.

In order to save disk space, a mask is now applied to images to keep only a small square around each Laue spot during thf-scans. Confluence pages describe the alignment method, measurement macros and analysis software. A publication describing the pseudomotor, the new setup, and codes, is in preparation.

The figures show 1) the multi-branch abacus, and 2) the dip curves on a Ge spot from 16 different diamond branches, illustrating typical accuracy of calibdia.

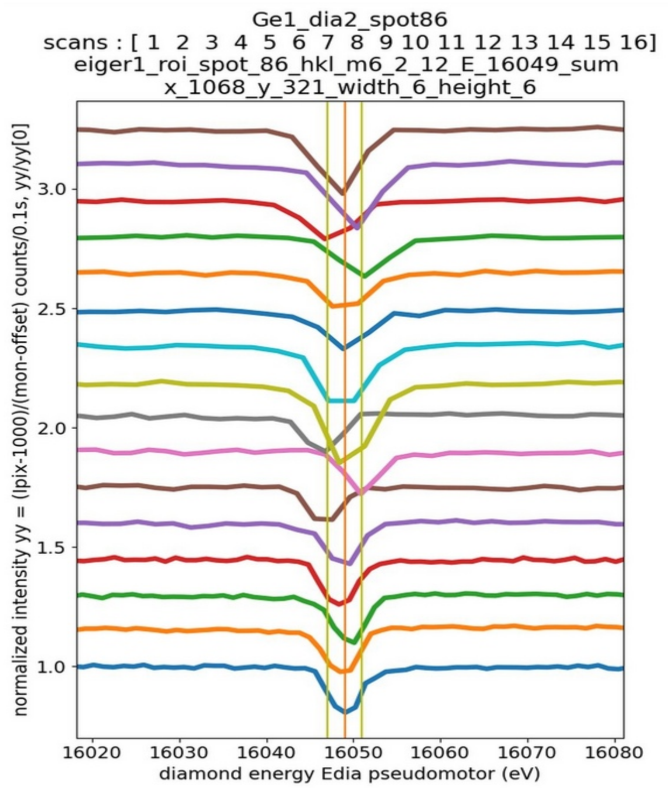

Figure IF-14: Intensity dip scans, cutting a Ge 16 keV Laue spot successively with 16 different {111} branches of the energy-angle abacus. Plotting versus Edia pseudo-counter allows superimposing curves measured at widely different thf angles. (blc15687 Sep24 BM02 Eiger)

Locating grain depth: DAXM - Wire-scanning

The use of wire-scanning on BM32 to obtain depth-resolution along the incident beam, via triangulation on diffracted beams, was first published by Hektor et al. in 2018, using analysis code developed by F. Grennerat (Post-Doc) then J.-B. Marijon (PhD). Further improvement of analysis software made by L. Renversade (PostDoc ANR-DFG XMicroFatigue lead by J.S. Micha and C. Kirchlechner, MPIE Düsseldorf) to include non-zero transmission at edges of scanning wire and linear minimisation method was finally published in 2024 by J.-B. Molin et al. Multi-wire scanning is now routinely available, with user-friendly notebooks for producing a depth-series of reconstructed Laue patterns, thanks to the work of C. Ribart (PostDoc). This is a successful example of beamline produced-code getting mastered by an external group of users (KIT, Kirchlechner, Fréville) and coming back improved to the beamline.

For strongly multi-grain Laue patterns, and samples with probe depth above 10 microns, depth-sorting of grains by DAXM improves accuracy on deviatoric strain and orientation, via better accuracy on Laue experimental geometry (reduced parallax errors).

Since 2025, a 3D-printed multi-wire holder is now supported by a motorized or manual rotation stage, to align wire shadow with the pixel rows of the 2D detector. This helps with a rapid evaluation of the DAXM scan quality (horizontal wire shadowing of detector pixel) by controlling the relative wire position difference between Laue spots dips of two grains at two different depths.

DAXM developments are foreseen to separate the wire-scanning stage from the sample holder stage, possibly by copying of the APS setup. Low-mechanical-resistance magnetic kinetic mounts for the wire holding stage would help reduce damage to sample and reduce rewiring time when the wire hits the sample by mistake. Analysis is still pending to check whether distorsion-correction of sCMOS detector impacts strain-versus-depth profiles.

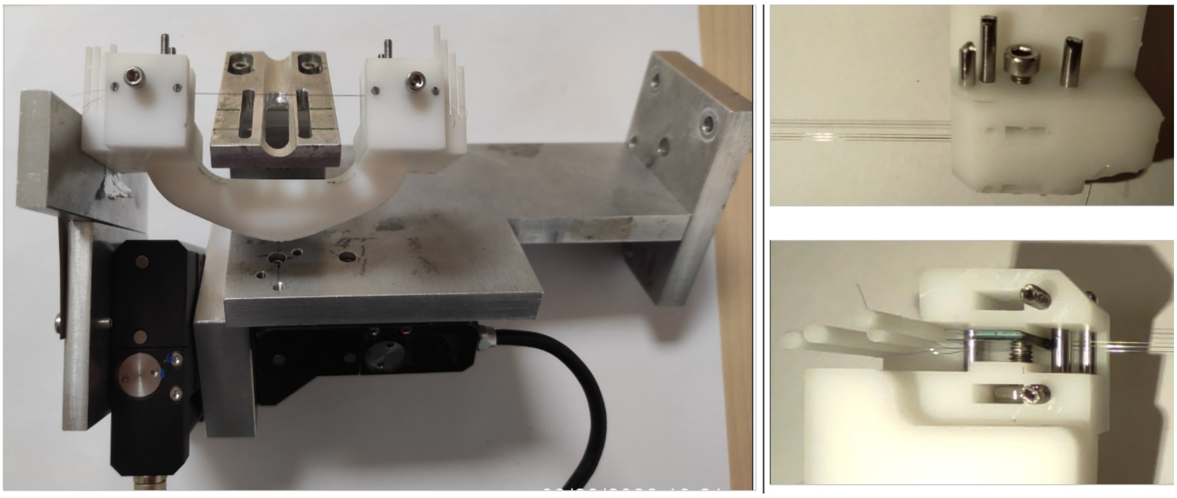

Left DAXM wire-scanning setup for depth-resolution along the incident beam. Right: since middle of 2025, the recent additive manufactured wires holder to adapt easily the number of wires and their mutual distance on purpose.

Softwares

On the closer side of the beamline needs, we developed several macros or software tools to accelerate alignments for a larger fraction of scientific measurements during the experimental run.

• Continuous- (fly-, fast-) Scanning (INS2, LaueMAX, GMT):

As mentioned earlier, we are continuing the conversion of motor scans from step-by-step mode (motor movement, motor stop for measurement) to continuous mode (or flyscan). In this latter mode, with no dead time, counters and detectors are synchronized by a counting card while motors traverse the path at a constant speed. The trajectory can be programmed using the coordinates of physical or virtual motors (combinations of motors). Continuous scans are extremely useful for alignments across all three instruments on the beamline. They can also be used for scientific measurements when the signal-to-noise ratio is sufficient, particularly for samples with strong diffraction.

• 'Sample Manager', Position Memorization, and Sample Holder Dismantling/Reassembly (LaueMAX):

By memorizing regions of interest on a standardized sample holder, we have developed a Python class *memposition* to calculate a coordinate transformation when dismounting and remounting a previously studied sample plate, allowing for quick relocation and alignment on pre-identified patterns. Similarly, we can offer a reference for the X and Y translation axes aligned with directions suitable for the orientation of a nanowire or a regular array of objects whose lattice vectors are slightly tilted due to mechanical play during the mounting and dismounting of sample holders.

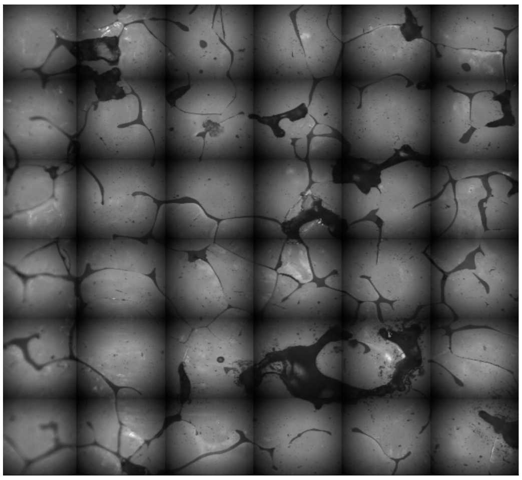

Surface mapping using a high-definition optical microscope (visible light) on a large scale (here, a 1.2 × 1.2 mm² field of view, with each pixel corresponding to 0.2 × 0.2 µm²), enabling the identification and memorization of regions of interest for subsequent serial measurements. Local elevation (topography) for each of the 36 sub-images is determined and recorded. The implementation of this measurement uses the home-developed Python class samplemap.

• *HKL* module (INS2, GMT):

Given that INS2 was the first diffractometer to be controlled in BLISS using the 'hkl' library developed at Soleil, the beamline staff significantly contributed to debugging the BLISS diffractometer class, enhancing its development to better meet user needs, and defining the most ergonomic scan and alignment functions.

The developments implemented on the beamline have been integrated into the latest versions of Bliss. Thanks to their hands-on experience, the BM32 staff also actively participated in the transition of other diffractometers at the ESRF to *BLISS*, including the 6-axis kappa diffractometer on BM02 and the 6-circle Eulerian diffractometer on BM28.

LaueMAX-related softwares

Started in 2009, the *LaueTools* suite is an open-source package of python written modules dedicated to the data analysis of Laue microdiffraction data (Laue pattern images). Whereas it was initially designed to facilitate the data handling on laptops, the main milestone during the 2020-2025 period was the easy access to parallel computing on HPC servers both for users at ESRF and for external users who would request to exploit their data remotely. Another game changer was the success of indexing complex Laue Pattern by training a Neural Network for the classification of Laue spot HKL class (*LaueNN*). To face the huge amount of data (peak value ~ 1 To/day) we also built optimized python classes for *pytorch* (and GPU) processing and careful usage of memory (*LaueImProc*).

The maintenance of these software tools remains challenging and time-consuming. Mainly through self-educated training, the support of fixed-term contracts engineers with IT skills, and the help of ESRF DAU and ADA groups, the beamline staff is able to maintain and distribute (with environment) scientific codes on repositories, some at a very advanced level in the algorithmic point of view. However, this maintenance is still demanding and non-optimal in order to benefit from software engineering standard development continuous integration codes, because it is done by staff whose available time for coding is limited.

In 2025, the main efforts were devoted to the acceleration of the LaueTools processing Laue pattern from polycrystalline materials including the integration of workflows for depth-resolved measurements (DAXM).

LaueTools

From 2024, we consolidated the analysis tools based on our HPC machine (256 CPUs labeled *jupyter-frcrg,* installed a year before) hosted at ESRF and funded by the annual beamline budget. This allows us and users to perform parallel calculations using *Jupyter* notebooks that call LaueTools modules for image processing and data extraction (reduction) in order to obtain a qualitative (but very informative) visualization of the maps measured by Laue microdiffraction. This extracted data can be saved for later viewing and interaction; we have therefore developed a reader/browser for this type of file in order to quickly browse all the extraction results without recalculating them. These notebooks can also perform the three classic steps of analysis on a set of images (peak search, indexing, and data refinement), while the graphical interface remains very useful for learning the technique and analyzing complex images or a limited series of images that are “too unusual” from the point of view of current automation tools.

Thanks to the presence of R. Richard, notebook workflows for frequently used analysis steps have been set up with a focus on clarity and ergonomics. These notebooks can run on a laboratory computer but take advantage of the computing power of machines hosted at the ESRF with 40 (nice server), 64 (*jupyter_frcrg*), or 144 CPUs (*lbm32gpu1* purchased and installed in 2024 in the framework of ANR-DFG HotMIX project). We also received the help of S. Bongiorno, B. Foschiani, and C. Ribart, for the steps of searching for diffraction peaks, indexing them, refining the structure, and post-processing to compile and visualize the values of the measured physical quantities (*LaueXplore*, to be submitted). Since Fall 2025, thanks to the MAGNIFIX project, 3 machines of 192 cores each, have formed an ESRF cluster partition called ‘MAGNIFIX’ with priority access, can be used to fast processing triggered by notebooks or scripts.

We have also added some estimates of the error bar on the strain values in 2025. The main contribution to the error bar is the probing depth, which varies between the different Laue spots, and can come from thick grains and/or buried ones at unknown depth. By refining the Laue pattern with a series of different probing depths, we can get a first estimate on the error bars on the strain and orientation components.

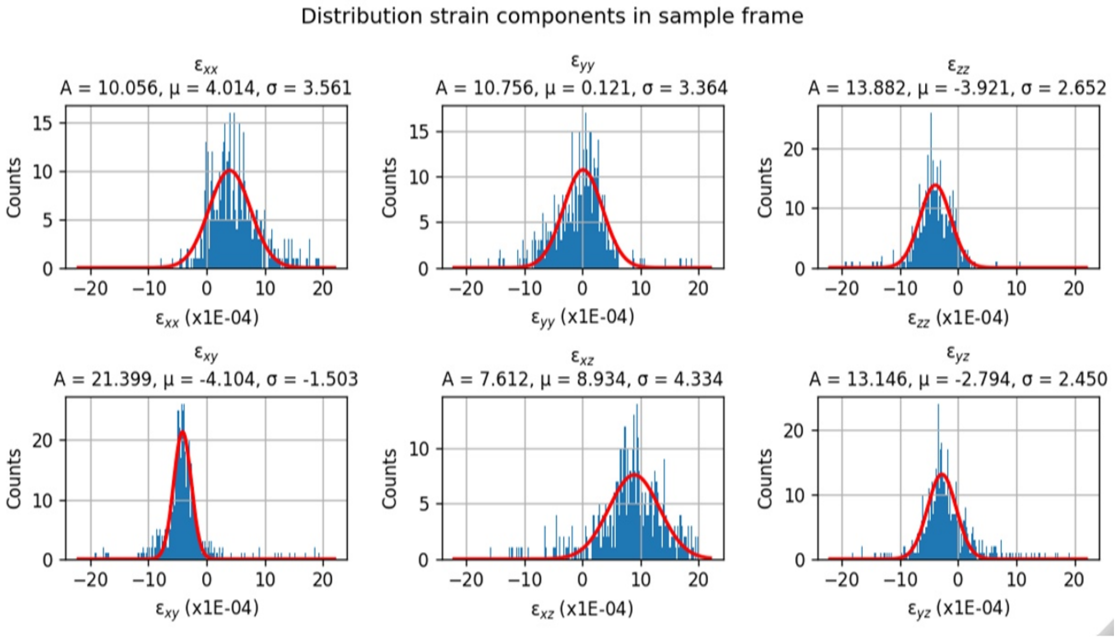

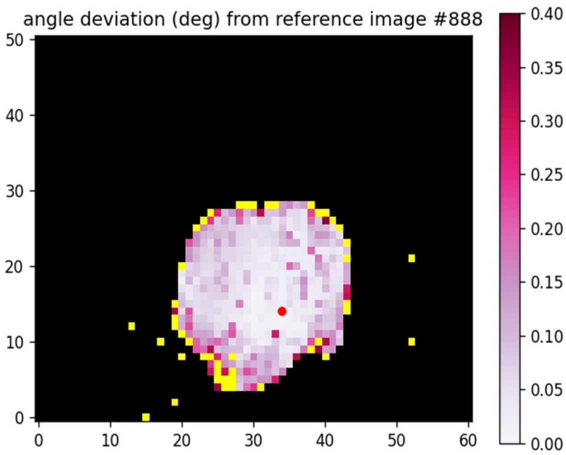

Figue IF-15: (top) distribution (blue histogram) of the value of deviatoric strains by component (here in the sample coordinate system) for the selected mapping regions (here a Zr grain from the following figure). The mean values and their standard deviations can be deduced (μ and σ).

(left): mapping of angular disorientation (in degrees) relative to the orientation at the centre of a Zr grain.

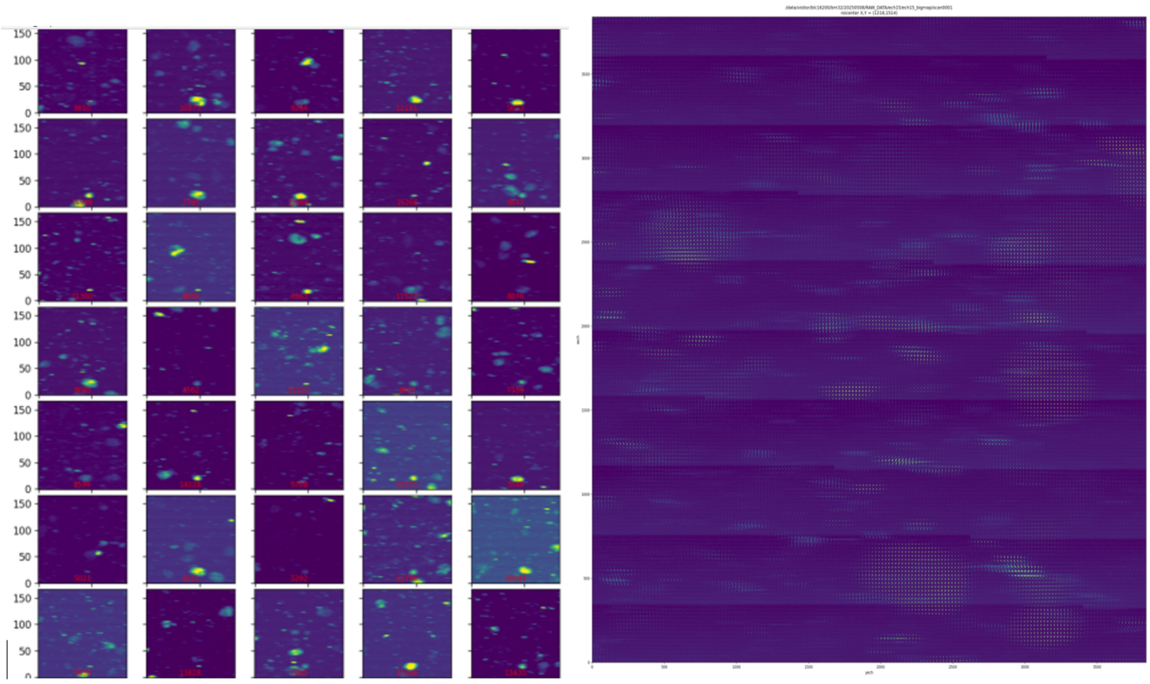

Figure IF-16: Tracking and localization of scattering grains or regions during or after the measurement campaign of polycrystalline microstructure. Regardless of the nature of the grains or their orientation, 2D Laue mapping can detect the crystals probed in a large field of view if necessary, or in the first 50 µm of depth for absorbing materials or 500 µm for light materials. Left: maximum intensity measured locally in 35 different ROIs of the Laue camera. Right: an extract of the same 21x21 pixel ROI, extracted from more than 10,000 mapping images, rearranged in the form of a mosaic. These typical maps obtained online during the experimental campaign and without any IT or crystallography expertises are crucial to guide the acquisition strategy and strengthen the users connection with their rich data.

INS2 : Binoculars

With the advent of 2D detectors for detecting surface diffraction signals, the possibility arose of “thinking before reducing data” instead of “reducing data first and thinking after”. Namely, we tried to exploit intensities from all pixels and not only roi intensities. This led to locally developed PyRod software (T. Zhou), typically used for integrating a series of azimuthal scans collected at different heights along a crystal truncation rod.

Several approaches to this same task were developed on various facilities and laboratories: with the aim of providing a common, standard reduced data file format and analysis tools to the community of surface diffraction, we adopted the “Binoculars” file format, in concert with the responsibles of SixS beamline at SOLEIL and i07 at Diamond light sources.

Binoculars is an ESRF (ID03)-developed software used to build 3D intensity maps in reciprocal space, from a series of scans, collected with a 2D detector. Its main function is converting real angles into reciprocal space coordinates, and converting measured intensities into “normalized intensities”, with “proper normalizing” for resolution function, geometrical and optical corrections… Binoculars first performs the conversion using a beamline-instrument-specific “backend” code. During this operation, it manages parallel processing of multiple scans. Afterwards, it dispatches the measured intensities and ‘contributions’ in voxels in reciprocal space.

We developed the backend for the INS2 diffractometer geometry and Bliss data format. The numerical optimization of the projection of 2D images to reciprocal space coordinates allowed for an improvement in data processing time by more than one order of magnitude compared to standard algorithms from general purpose libraries like PyMCA or XrayUtilities.

Data processing speed achieved on an Intel Xeon Platinum 8452Y workstation, starting from GZ compressed images, is around 5 Gpx/min.

GMT: XRR inversion

An effort has been made to provide the community with online resources for processing X-ray reflectivity (XRR) data. While many free and open-source XRR analysis packages exist, we are specifically providing the GenX software [A. Glavic and M. Björck J. Appl. Cryst. 55, 1063-1071 (2022)], along with Jupyter notebooks for data pre-processing. Additionally, we have developed tutorials for the Hercules school and Master's degree practical sessions, building a theoretical and pedagogical foundation accessible to all users.

In the specific case of studying symmetric interfaces, F. Rieutord demonstrated that the classic phase-retrieval problem could be reduced to a simple sign problem [D. Rébiscoul et al., Journal of Colloid and Interface Science 614, 396-404 (2022)]. Because an electron density profile that is symmetric around a central point possesses an antisymmetric gradient (described by an odd function), its transform is purely imaginary. Consequently, to change sign, the amplitude must necessarily pass through zero. F. Rieutord authored an IgorPro code to perform this XRR curve inversion. With his assistance, a more sustainable and accessible Python alternative has been developed.

Jupyter notebooks have been developed with Z. Lu, allowing for the rapid inversion of reflectivity curves into an average electron density profile along the surface normal, immediately following acquisition. In a study on channel etching, this on-the-fly analysis made it possible to identify the fabrication parameters that produce channels with the appropriate shape and homogeneity for future in situ microfluidic transport studies. Integration into the ESRF EWOKS system was recently tested and validated in February 2026, with aim to provide a user-friendly direct data processing in BLISS.

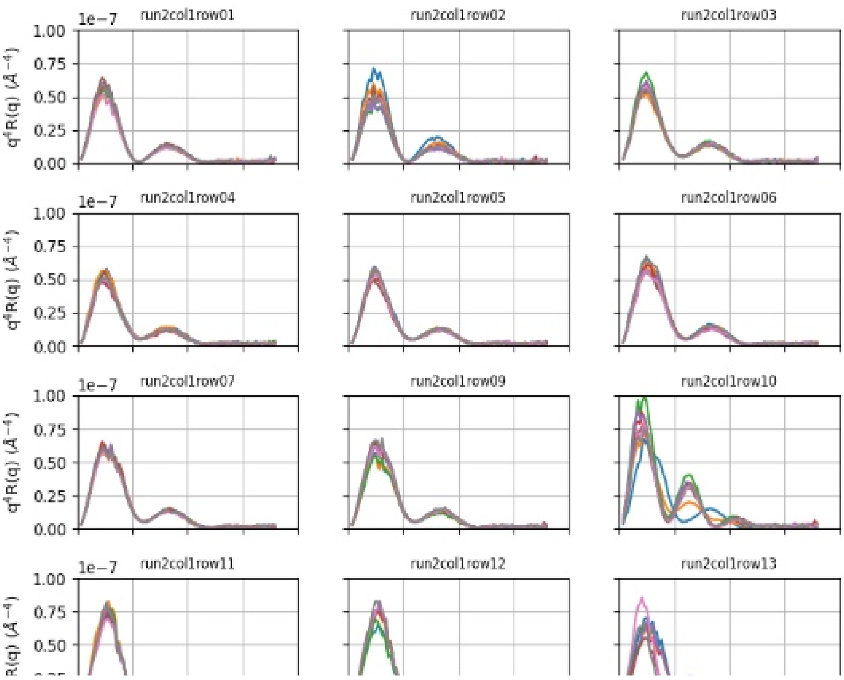

X-ray reflectivity spectra (reflected intensity R(q) as a function of the momentum transfer q, which is proportional to ϑ, where ϑ is the angle of incidence) measured on a "sample matrix" (here 4x4 samples, 12 *samples shown) at 27 keV on the GMT. The acquisition time is on the order of ten minutes, while positioning and alignment times (incidence zeroing) are under one minute, thanks to the controlled layout and pre-positioning.*

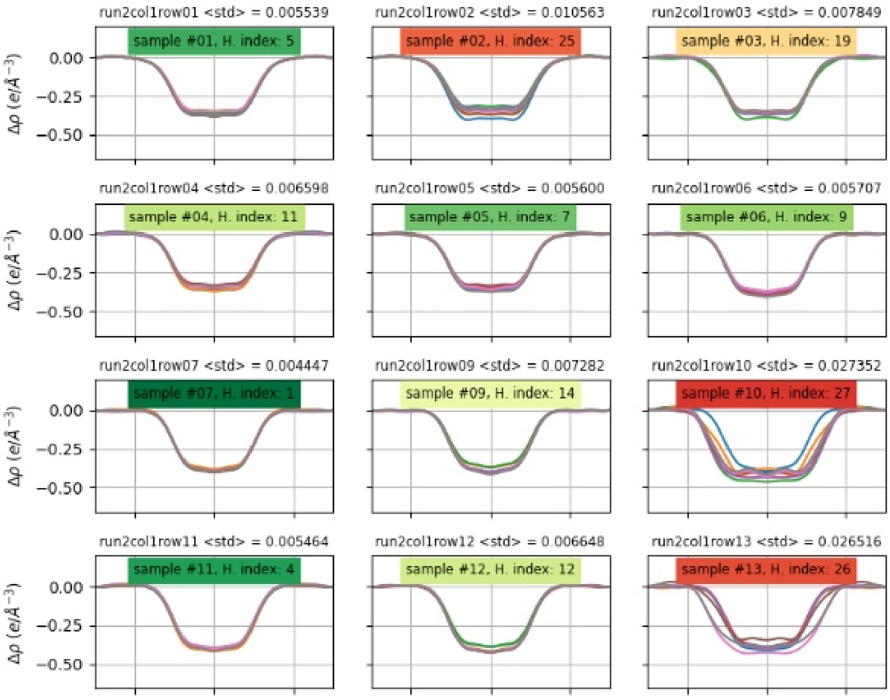

Electron density profiles at the interface between two silicon (Si) wafers with etched surface-channels. A simple indicator representing the dispersion of results across 12 different positions allows for the rapid selection of the best channels for microfluidic transport.

ACTIVITÉS SCIENTIFIQUES DES LIGNES

LIGNE IF «Interfaces» (BM32)

1. Faits scientifiques marquants

Nous avons sélectionné trois travaux récemment menés ou publiés en 2025 sur les trois instruments de la ligne IF. Pour

INS2: Structure of TiO_2 anatase (001) films grown on $SrTiO_3$(001) and $LaAlO_3$(001) by PLD and MBE.

X. Torrelles[1], M. De Santis[2], A. Crespo[1], M. Mosqueda[1], T. D. Dzeubou[2], V. Langlais[3], G. Cabailh[4]

[1] Institute of Materials Science of Barcelona (ICMAB-CSIC), Barcelona, Spain

[2] Université Grenoble Alpes, CNRS, Grenoble INP, Institut Néel, Grenoble, France

[3] Centre d'Elaboration de Matériaux et Etudes Structurales (CEMES-CNRS), Toulouse, France

[4] Sorbonne Université, UMR CNRS 7588, Institut des Nanosciences de Paris, Paris, France

Hydrogen is widely regarded as one of the most promising clean energy vectors for a sustainable energy future, provided it can be produced efficiently from water using renewable resources. Among the different routes under intense investigation, photocatalytic water splitting remains particularly attractive because it offers the prospect of directly converting solar energy into chemical fuel. However, the realization of efficient photocatalytic systems critically depends on identifying robust semiconductors that combine chemical stability, suitable band energetics, and efficient charge separation at the surface.

Among oxide photocatalysts, titanium dioxide (TiO_2) continues to stand out as a benchmark material owing to its exceptional chemical stability, earth abundance, non-toxicity, and low cost. Yet, despite decades of research, its practical performance remains limited by two well-known intrinsic bottlenecks: a wide bandgap (~3.2 eV in anatase), which restricts absorption largely to the ultraviolet, and the short lifetime of photogenerated electron–hole pairs, which leads to rapid recombination and poor solar-to-chemical conversion efficiency.

Not all TiO_2 surfaces are equally active. Among the three main TiO_2 polymorphs—rutile, anatase, and brookite—the anatase (001) surface is widely considered one of the most reactive and potentially one of the most photocatalytically active terminations. This enhanced activity originates from its high density of undercoordinated surface atoms and broken bonds compared with the thermodynamically dominant anatase (101) surface. While the (101) facet is the most stable and therefore the most commonly exposed in natural crystals and conventional nanostructures, the (001) surface is metastable, structurally demanding, and considerably more difficult to prepare in a well-ordered form. This synthetic difficulty has long limited direct structural determination of its reconstructed surface at the atomic scale.

A series of surface-sensitive diffraction experiments were performed on the INS2 beamline to address this challenge and determine the atomic structure of anatase TiO_2(001) thin films prepared by two complementary growth routes: pulsed laser deposition (PLD) in Barcelona and molecular beam epitaxy (MBE) at the Institut Néel in Grenoble. Initial X-ray reflectivity (XRR) measurements confirmed the successful growth of highly oriented anatase films. The specular diffraction signal displayed the characteristic anatase (004) reflection, demonstrating that the films were predominantly oriented along the [001] direction (Fig. 1a). Figure 1b shows grazing-incidence X-ray diffraction (GIXRD), probing the in-plane lattice, further revealed epitaxial growth and showed that the in-plane lattice parameter of the TiO_2 layer relaxes toward the anatase bulk value when grown on $SrTiO_3$-based templates.

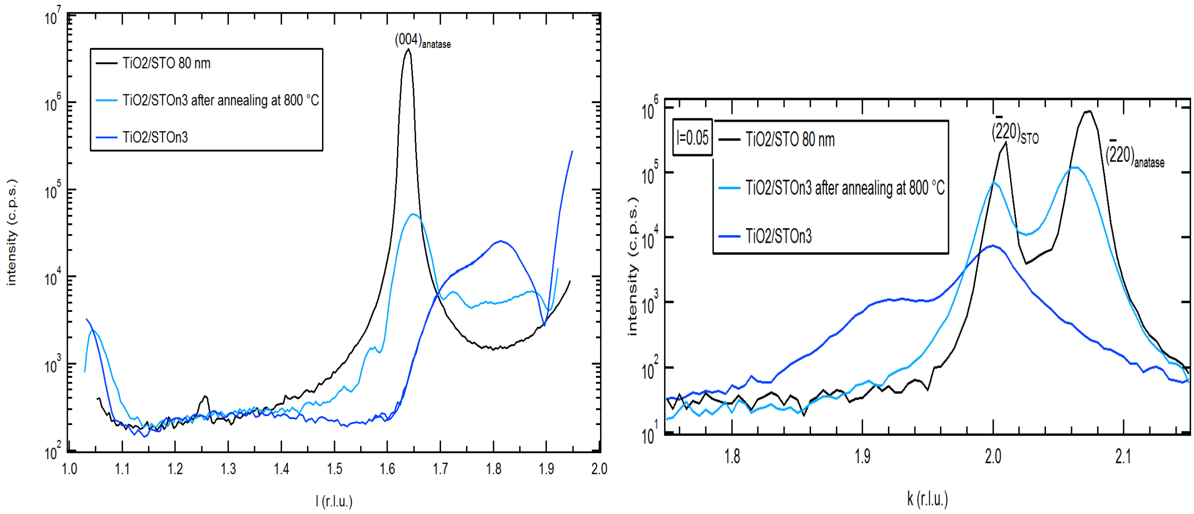

Figure 1. a) XRR of epitaxial titanium oxide layers on STO; b) GIRXD. Black: PLD growth. Dark blue: in situ measurement of a layer grown by MBE. Light blue: the same layer after ex situ annealing in O_2 at atmospheric pressure.

Because photocatalytic functionality is governed not only by bulk crystallinity but by the atomic-scale structure of the surface, the anatase layers were subsequently cleaned in situ by gentle Ar^+ sputtering followed by annealing at 850 °C under 10^{-6} mbar of O_2. Auger electron spectroscopy confirmed the absence of residual contaminants after treatment. Under these conditions, low-energy electron diffraction (LEED) revealed a well-ordered p-(4×1) reconstruction (Fig. 2), present in two orthogonal domains, for both PLD- and MBE-grown anatase (001) films. Although this reconstruction had been reported previously in the literature, its detailed atomic structure had remained unresolved.

Solving the structure of the anatase TiO_2(001)-(4×1) surface proved exceptionally challenging. Three

Figure 2 . LEED of a 8-nm-thick MBE grown anatase film.

Figure 3. LEED of TiO_2(001)-(4x1)/$LaAlO_3$(001) collected at 40 eV, 80 eV et 150 eV.

experimental campaigns on INS2 were required to obtain a sufficiently complete diffraction data set. The main difficulty was the intrinsically weak intensity of the superstructure rods associated with the reconstruction. This weakness is physically meaningful: the reconstruction is driven primarily by subtle rearrangements involving oxygen vacancies and near-surface relaxations, while oxygen contributes only weakly to the X-ray scattering signal. In addition, when anatase is grown on substrates with large lattice mismatch, such as $SrTiO_3$-based systems, the limited lateral coherence of TiO_2 domains further reduces the sharpness and intensity of the superstructure features. These two factors together—weak oxygen sensitivity in X-ray diffraction and structural broadening from imperfect epitaxy—made direct structural refinement particularly demanding.

A decisive breakthrough was achieved by shifting to anatase TiO_2(001) grown on $LaAlO_3$(001). In this heterostructure, the smaller lattice mismatch enables coherent epitaxial growth, significantly improving the structural perfection of the film and, crucially, the long-range order of the reconstructed surface. The improvement is immediately visible in LEED (Fig. 3), where the p-(4×1) pattern becomes sharper and more intense, indicating larger reconstructed domains and better surface coherence.

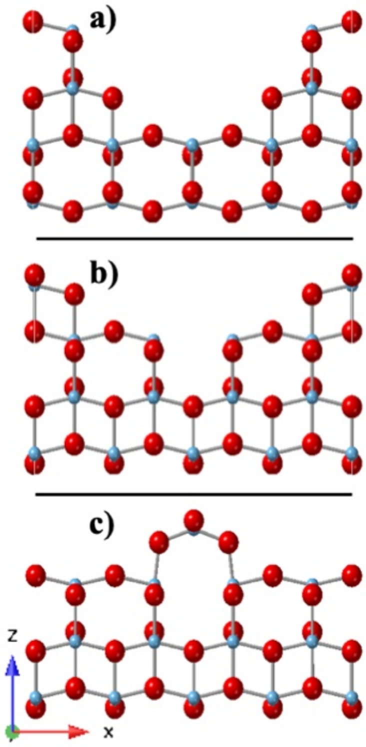

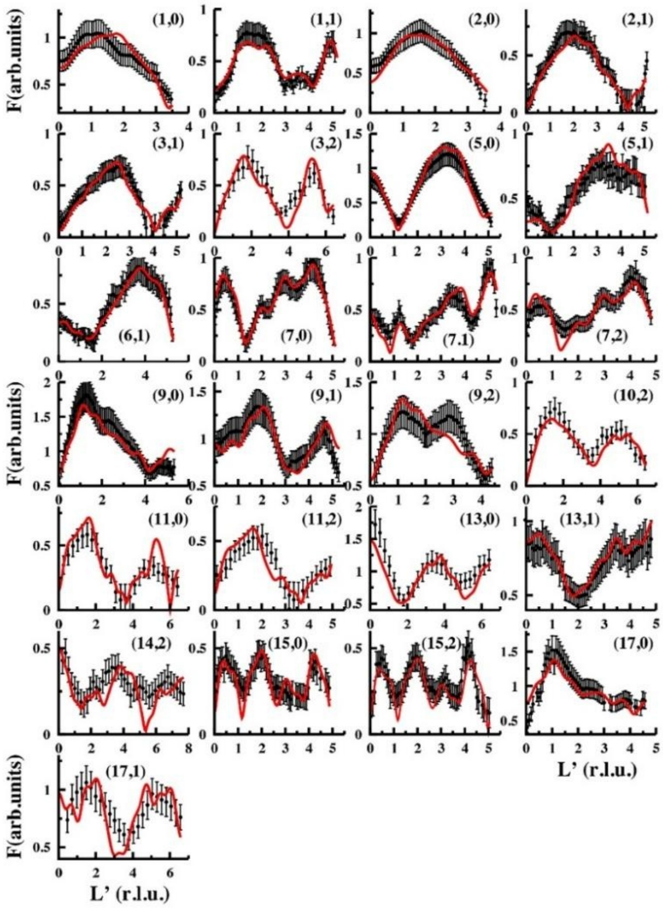

Fig. 4 anatase (001)-p4x1 models.

Figure 5 Best fit of superstructure rods

This enhanced structural quality provided, for the first time, a sufficiently robust set of surface X-ray diffraction data to discriminate between competing structural models (Fig. 4). From these coherently grown films, a comprehensive set of superstructure rods could be measured and indexed in the (4×1) surface lattice (Fig. 5). Several candidate structural models were tested against the experimental diffraction intensities. Comparison between measured and calculated rod profiles clearly identified model c as the best description of the anatase TiO_2(001)-(4×1) reconstruction. The agreement between experiment and refinement across the superstructure rods provides strong evidence that the p-(4×1) ordering arises from a specific, reproducible vacancy-mediated surface rearrangement rather than from a disordered defect ensemble.

Beyond the structural solution itself, the result has broader implications for photocatalysis and oxide surface science. The anatase (001) facet is often invoked as a highly active surface in photocatalytic studies, yet its actual atomic structure under realistic preparation conditions is rarely known with certainty. This work closes that gap by providing a direct structural benchmark for a technologically relevant and catalytically important surface. It also demonstrates that interfacial and epitaxial design are not merely growth parameters, but enabling tools for accessing metastable functional oxide surfaces that are otherwise difficult to characterize. In particular, coherent epitaxy on $LaAlO_3$(001) stabilizes the anatase TiO_2(001) phase while simultaneously enhancing the long-range order required for quantitative structural refinement of the p-(4×1) reconstruction.

The study therefore establishes a crucial structure–stability–function link.

To understand and ultimately optimize photocatalytic TiO_2(001), one must first stabilize the surface in a structurally coherent form, then resolve its reconstruction at the atomic scale. This work provides that foundation. It opens the way for future investigations of how the reconstructed anatase (001) surface controls adsorption, charge separation, oxygen vacancy chemistry, and ultimately photocatalytic performance in water splitting and related solar-fuel reactions.

The results of these studies are submitted for publication.

LAUE: Multimodal Imaging of Strain and Light Emission of Core–Shell InGaN/GaN Wires under a Sub-Micrometer Polychromatic X-Ray Probe

B. de Goes Foschiani[a], S. Bongiorno[a], O. Robach[a], O. Ulrich[a], J.-S. Micha[b], J. Eymery[a]

Advanced Materials Interfaces 13, e01025 (2026) https://doi.org/10.1002/admi.202501025

[a] Univ. Grenoble Alpes, CEA, IRIG, MEM, NRX, Grenoble, France

[b] Univ. Grenoble Alpes, CNRS, UMR SyMMES, CEA-Grenoble/IRIG, France

This study, performed during the PhD work of Beatriz de Goes Foschiani, presents a multimodal characterization approach combining micro-Laue (µLaue) X-ray diffraction and X-ray excited optical luminescence (XEOL) to simultaneously map local strain, crystal orientation, and light emission in core-shell InGaN/GaN multiple quantum well (MQW) wires. Using a sub-micrometer polychromatic X-ray probe and the LaueMax setup, the components of the deviatoric strain tensor for both the GaN core and the InGaN/GaN shell can be quantified independently, achieving a measurement precision better than 9×10^{-5} and an accuracy of approximately 4×10^{-4}.

The structural analysis revealed that the strain is tensile along the -c-axis and compressive in the perpendicular plane, findings that were validated by 3D finite element method (FEM) simulations. Correlated XEOL hyperspectral mapping identified several emission contributions: a dominant UV-blue MQW emission from the nonpolar m-planes, a secondary emission from semipolar r-plane facets (~470 nm), the GaN near-band-edge signal (~363 nm), and yellow defect-band luminescence (560 nm). Notably, a progressive wavelength blue-shift (from 406 nm to 397 nm) was observed along the wire axis, which is attributed to a linear gradient in indium composition (ranging from 10% to 8%) rather than strain effects.

Unlike conventional electron-based microscopy, this synchrotron-based approach provides a non-destructive, bulk-sensitive investigation of strain–light coupling mechanisms. The study demonstrates the technique's potential for high-throughput screening, process optimization, and the rational design of next-generation optoelectronic nanodevices. It has been recently published in 2026.

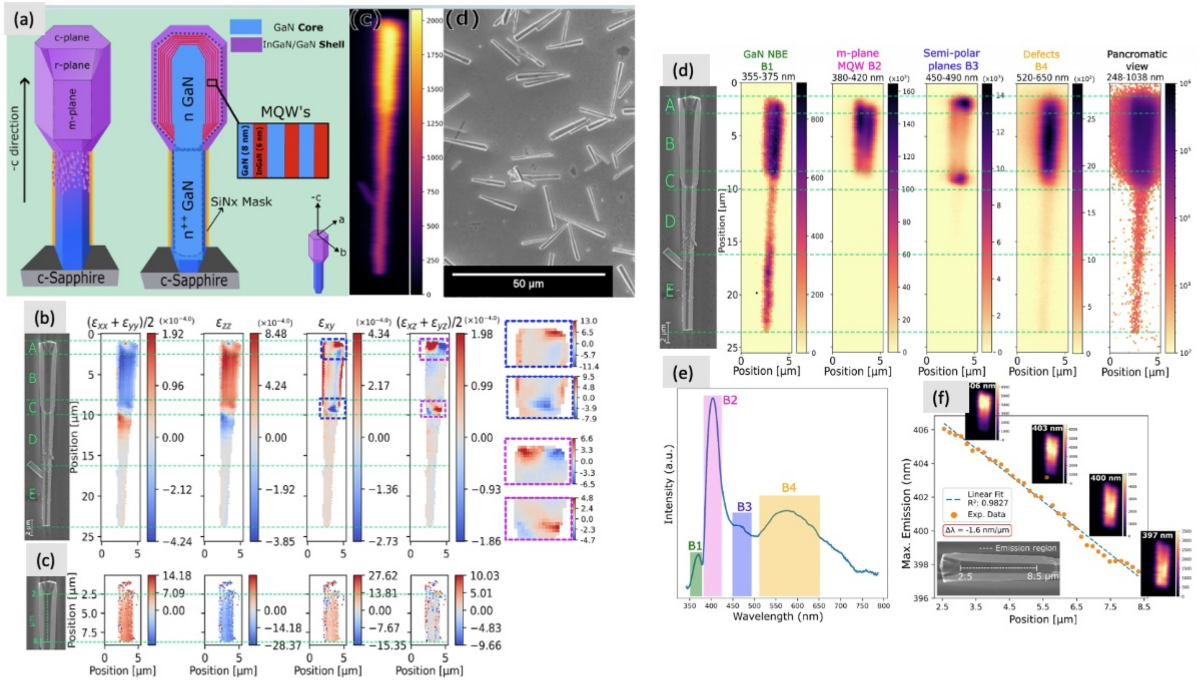

Figure 1. (a) Schematic of the GaN microwires with Inx Ga1-x N/GaN core–shell multiple quantum wells at the top of the structure, GaKα fluorescence mapping and Scanning electron microscopy of dispersed wires. (b-c) Deviatoric strain maps of GaN core and InGaN/GaN MQW shell. (d) XEOL emission maps for different wavelength ranges (2.25 s counting time, 5.3×25.5 µm^2,31×151 steps). (e) Panchromatic luminescence. (f) details the analysis of the m-plane MQW emission.

GMT: Industrial processes in wafer-bonding investigated by X-ray Reflectivity

Mechanisms of sodium hydroxide (NaOH)-catalyzed sealing of SiO2/SiO2 direct bonding interfaces

P. Noel[1], F. Rieutord[2], V. Larrey[1], S. Tardif[1], C. Morales[1], H. Hijazi[1], V. Thoréton[1], A.-M. Papon[1], Z. Saghi[1], D. Landru[2], F. Fournel[1]

J. Appl. Phys. 138, 055307 (2025) https://doi.org/10.1063/5.0277335

Thin dielectric to dielectric hydrophilic wafer bonding for FD-SOI and C-FET manufacturing

P. Noel[1], V. Larrey[1], S. Tardif[1], F. Rieutord[2], D. Landru[2], F. Fournel[1]

Solid-State Electronics 229 (2025) 109188 https://doi.org/10.1016/j.sse.2025.109188

Hydroxide and fluoride catalyzed bonding interface closure for low-temperature wafer bonding

P. Noel[1], V. Larrey[1], S. Tardif[1], F. Rieutord[2], D. Landru[2], F. Fournel[1]

[1] Univ. Grenoble Alpes, CEA-Grenoble, Grenoble, France
[2] SOITEC, Parc Technologique des Fontaines, 38190 Bernin, France

Japanese Journal of Applied Physics 64, 03SP06 (2025) https://doi.org/10.35848/1347-4065/adb6af

In collaboration with CEA-Leti (PhD of Paul Noel), we have explored the chemical mechanisms that enable high-energy SiO2/SiO2 direct bonding at low thermal budgets, a requirement for advanced semiconductor applications like FD-SOI and C-FET manufacturing.

By introducing catalysts such as sodium hydroxide (NaOH), cesium fluoride (CsF), or ethanolamine via spin-drying prior to bonding, we achieved bonding energies reaching the silicon fracture level (~5 J/m²) at temperatures as low as 250°C—significantly outperforming standard de-ionized water (DIW) references.

The electron density profiles extracted from HXRR data were instrumental in revealing the unique morphology of catalyzed interfaces (Fig. 1). XRR allowed us to observe that NaOH-prepared samples exhibit higher gap densities (reaching ~0.53 e-/Å³) compared to DIW references (~0.45 e-/Å³) at 100°C, indicating a faster initial sealing. XRR results also evidenced a significant widening of the interface gap as annealing temperatures increased to 300°C for catalyzed samples, which we interpret as the formation of interfacial water nanoclusters (or nanobubbles). This highlights the critical competition between accelerated interface sealing (driven by the catalyst) and water out-diffusion into the oxide. Because the catalyst speeds up the formation of covalent bonds, water becomes trapped and concentrates into incompressible droplets before it can diffuse away, eventually compromising the interface. XRR data also revealed that thinner oxides (10 nm) act as smaller reservoirs for water, leading to larger nanoclusters and wider interfaces compared to thicker oxides (100–500 nm), which can better absorb interfacial water.

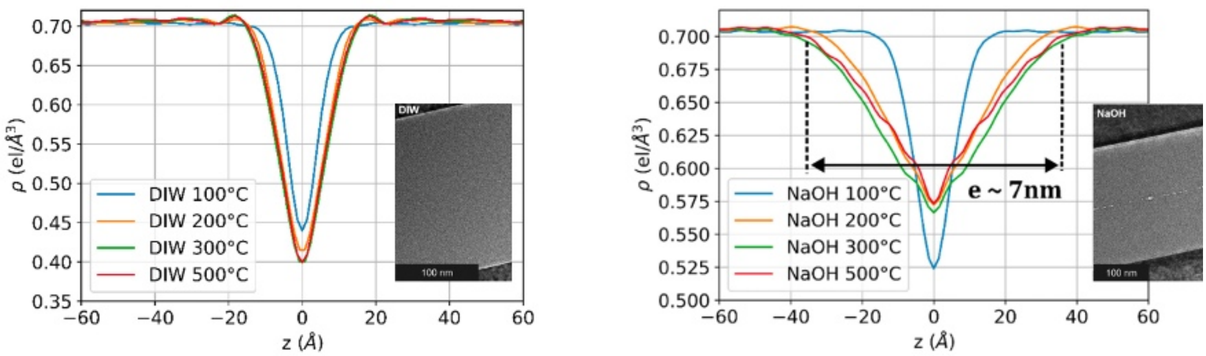

Figure.1. Electron density profile of the DIW (left) and NaOH (right) bonding interface for 100, 200, 300, and 500 °C anneals (2 h–100 nm thick oxides). The insets are cross-sectional TEM imaging of SiO2/SiO2 interfaces after DIW and NaOH surface preparation, bonding, then 300 °C annealing for 2 h.

Our results suggest that the catalysis occurs via a nucleophilic attack by OH^- or F^- ions on silicon atoms. This attack creates unstable reaction intermediates that enhance the rates of both silanol condensation (forming Si-O-Si bonds) and silica hydrolysis (softening surface asperities to allow better contact). We confirmed these XRR-derived findings through complementary Transmission Electron Microscopy (TEM), which visually identified the ~7 nm clusters predicted by our density profiles, and ToF-SIMS, which tracked the water (OH) and catalyst (Na) distribution.

In conclusion, our work demonstrates that while catalyzed bonding creates an interface that may appear "defective" due to nanoclusters, it provides superior mechanical coherence at low temperatures. XRR remains the essential technique for designing these interfaces, as it uniquely captures the balance between chemical sealing and water management.

2. Production scientifique (à partir de 2024)

Nous listons ci-après les articles publiés depuis 2024. Depuis quelques années, une dizaine d'articles (certains à fort impact) sont publiés par an.

Revue à comités de lecture

Balisage par type d'expérience :

[IHR] IHR: travaux conduits par un ou plusieurs membres de la ligne (expérience(s) réalisée(s) sur du temps IHR ou sélectionné par comités de programme)

[C] Travaux collaboratifs :au moins une personne sur la liste des auteurs (expérience(s) réalisée(s) sur du temps IHR ou sélectionné par comités de programme)

[U] Travaux menés par les utilisateurs externes (pas de contribution notoire du personnel de ligne)

Balisage par instrument :

[LAUE] Microdiffraction sur LaueMAX (cabane EH1)

[GMT] Goniomètre multitechnique (cabane EH2)

[INS2] Chambre UHV et Diffractomètre (cabane EH3)

[ ] *Impact factor* du journal en 2024 d'après J. cit. reports™

() nombre de citations (février 2026)

2026

[IHR][LAUE][4.4] *Multimodal Imaging of Strain and Light Emission of Core–Shell InGaN/GaN Wires under a Sub-Micrometer Polychromatic X-Ray Probe,* B. de Goes Foschiani, S. Bongiorno, O. Robach, O. Ulrich, J.-S. Micha, J. Eymery,

Advanced Materials Interfaces 13, e01025 (2026) https://doi.org/10.1002/admi.202501025

[U] [LAUE] [6.6] *In situ Laue microdiffraction tracking of the {110} to {112} slip mode transition in L21-ordered MnCu2Al,* Rhodes B.E., Comby-Dassonneville S., Cornelius T.W., Thomas O., Beyerlein I.J., Gianola D.S.,

Journal of Materials Research and Technology 41, 6748-6765 (2026)

https://doi.org/10.1016/j.jmrt.2026.02.172

Residual stress in Germanium single crystals caused by femtosecond laser micromachining,

[C] [LAUE] [2.9] Fréville R., Gruber P.A., Lee S., Micha J.-S., Robach O., Ulrich O., Kirchlechner C.

Materialia, 102648 https://doi.org/10.1016/j.mtla.2025.102648

2025

(4) Real-time helium bubble growth in tungsten by in-situ GISAXS

[U] [INS2] [2.7] Corso L., Curiotto S., Cheynis F., Müller P., Bernard E., Cabié M., Martin C., Leroy F., Nuclear Materials and Energy 42, 101894 (2025) https://doi.org/10.1016/j.nme.2025.101894

(2) High temperature evolution of interfacial metal film bonding two 4H-SiC substrates

[U] [GMT] [6.9] Le Cunff M., Rieutord F., Landru D., Kononchuk O., Cherkashin N., Applied Surface Science 682, 161678-1-161678-12 (2025) https://doi.org/10.1016/j.apsusc.2024.161678

(6) Formation and evolution of the solid electrolyte interphase on silicon electrodes from fluorine-free electrolytes

[IHR] [GMT] [12.1] Lu Z., Patranika T., Naylor Andrew J., Mindemark J., Tardif S., Hernandez G., Lyonnard S., Small 21, 2410654 (2025) https://doi.org/10.1002/smll.202410654

(4) In-situ Laue micro-diffraction during compression tests on Ce-TZP single crystal micropillars

[C] [LAUE] [6.2] Magalhaes M.D., Douillard T., Reveron H., Comby-Dassonneville S., Cornelius T.W., Meille S., Texier M.,Micha J.S., Rodney D., Thomas O., Chevalier J., Journal of the European Ceramic Society 45, 116794-1-116794-9 (2025) https://doi.org/10.1016/j.jeurceramsoc.2024.116794

(3) Hydroxide and fluoride catalyzed bonding interface closure for low-temperature wafer bonding

[U] [GMT] [1.8] Noel P., Larrey V., Tardif S., Rieutord F., Landru D., Fournel F., Japanese Journal of Applied Physics 64, 03SP06-1-03SP06-5 (2025) https://doi.org/10.35848/1347-4065/adb6af

Toward the Identification of Point Defects Formation and Solution Growth Mechanisms ofHerbertsmithite $Zn_xCu_{4-x}(OH)_6Cl_2$ Crystals

[C] [LAUE] [3.4] Paul Raj V.S., Pena-Revellez A., Micha J.S., Purushottam Raj Purohit R.R.P., Chaussende D., Verdier M.,Motto-Ros V., Bert F., Mendels P., Montes-Hernandez G., Velazquez M., Crystal Growth & Design 25, 2857-2873 (2025) https://doi.org/10.1021/acs.cgd.4c01483

(4) Reactive molecular beam epitaxy growth of a 1T-FeS2 single-layer–atomic structure, Moiré, and decoupling via intercalation

[IHR] [INS2] [16.1] Prabhu M.K., David P., Guisset V., Martinelli L., Coraux J., Renaud G., ACS Nano 19, 13941-13951 (2025) https://doi.org/10.1021/acsnano.4c17873

(2) Eutectic grains and orientation relationships in thin directionally solidified Al-Al2Cu samples: A Laue micro-diffraction study,

[C] [LAUE] [6.3] Medjkoune M., Bottin-Rousseau S., Carroz L., Soucek R., Prévot G., Croset B., Micha J.-S., Akamatsu S., J. Alloys and Compounds 1036, 181841 ttps://doi.org/10.1016/j.jallcom.2025.181841

Three-point bending behavior of individual ZnO nanowires studied by in situ Laue microdiffraction

[U] [LAUE] [2.8] Saïdi S., Texier M., Sharma S., Ardila G. Ternon C., Micha J.-S., Escoubas S., Thomas O., Cornelius T.W., Journal of Applied Crystallography 58, 1149-1158 (2025) https://doi.org/10.1107/S1600576725003668

Thin dielectric to dielectric hydrophilic wafer bonding for FD-SOI and C-FET manufacturing

[C] [GMT] [1.4] Noel P., Larrey V., Tardif S., Rieutord F., Landru D., Fournel F., Solid State Electronics 229 (2025) 109188 https://doi.org/10.1016/j.sse.2025.109188

Mechanisms of sodium hydroxide (NaOH)-catalyzed sealing of SiO_2/SiO_2 direct bonding interfaces,

[U] [GMT] [2.5] Noel P., Rieutord F., Larrey V., Tardif S., Morales C., Hijazi H., Thoréton V., Papon A.-M., Saghi Z., Landru D., Fournel F., Journal of Applied Physics 138, 055307 (2025), https://doi.org/10.1063/5.0277335

2024

(1) Polarization structure of nanostrip domain intersections in GeTe films

[U] [INS2] [3.7] Croes B., Cheynis F., Cherifi-Hertel S., Dorkenoo K.D., Müller P., Curiotto S., Leroy F., Physical Review B 109, 024103-1-024103-9 (2024) https://doi.org/10.1103/PhysRevB.109.024103

(35) Strain and collapse during lithiation of layered transition metal oxides: a unified picture

[IHR] [GMT] [31] Jousseaume T., Colin J.F., Chandesris M., Lyonnard S., Tardif S., Energy & Environmental Science 17, 2753-2764 (2024) https://doi.org/10.1039/D3EE04115H

(5) High temperature evolution of a confined silicon layer

[U] [GMT] [2.5] Le Cunff M., Rieutord F., Landru D., Kononchuk O., Cherkashin N., Journal of Applied Physics 135, 245301-1-245301-13 (2024) https://doi.org/10.1063/5.0205878

(6) Probing surface dynamics of SiOx thin-film electrodes during cycling through X-ray photoemission spectroscopy and operando X-ray reflectivity

[IHR] [GMT] [8.2] Lu Z., Zrikem K., Le Cras F., Tanaka M., Nakamoto M., Benayad A., Tardif S., van Roekeghem A., ACS Applied Materials & Interfaces 16, 52130-52143 (2024) https://doi.org/10.1021/acsami.4c05078

(1) Intermitted 3D diffraction tomography combined with in situ Laue diffraction to characterize dislocation structures and stress fields in microbending cantilevers

[C] [LAUE] [3.3] Molin J.B., Renversade L., Micha J.S., Ulrich O., Robach O., Gruber P.A., Kirchlechner C., Advanced Engineering Materials 26, 2400357-1-2400357-12 (2024) https://doi.org/10.1002/adem.202400357

(3) Electrical activation of insulator-to-metal transition in vanadium dioxide single-crystal nanobeam and their high-frequency switching performances

[C] [LAUE] [2.5] Orlianges J.C., Allegret O., Sirjita E.N., Masson A., Boulle A., Théry V., Tardif S., Micha J.S., Crunteanu A., Journal of Applied Physics 136, 064502 -1-064502 -7 (2024) https://doi.org/10.1063/5.0221152

(3) Laue microdiffraction on polycrystalline samples above 1500 K thanks to the QMAX-microLaue furnace

[IHR] [LAUE] [2.8] Purohit R.R.P.P.R., Fowan D., Arnaud S., Blanc N., Micha J.S., Guinebretière R., Castelnau O., Journal of Applied Crystallography 57, 470-480 (2024) https://doi.org/10.1063/5.0221152

(4) Preferential orientations of FeRh nanomagnets deposited on a $BaTiO_3$ epitaxial thin film

[C] [INS2] [3.7] Reyes A., Herrera G., Capiod P., Le Roy D., Dupuis V., Cañero-Infante I., Saint-Girons G., Bachelet R., Resta A., Ohresser P., Martinelli L., Weng X., Renaud G., Tournus F., Physical Review B 109, 245410-1-245410-9 (2024) https://doi.org/10.1103/PhysRevB.109.245410

(2) Energy-dispersive Laue diffraction analysis of the influence of statherin and histatin on the crystallographic texture during human dental enamel demineralization

[C] [LAUE] [2.8] Sakr C., Al-Mosawi M., Grünewald T.A., Cook P., Tack P., Vincze L., Micha J.S., Anderson

P., Al-Jawad M., Lichtenegger H.C., Journal of Applied Crystallography 57, 1514-1527 (2024) https://doi.org/10.1107/S1600576724007180

Thèses

Catalysis effect in direct bonding mechanisms

Noël P.

Université Grenoble Alpes, Grenoble, France (PhD thesis), 2025

Transformation-induced plasticity in ceria-doped zirconia ceramics at small scales

Demetrio de Magalhaes M.

Université de Lyon, France ((PhD thesis), 2025

Evolution cristalline du tungstène sous irradiation hélium: formation et évolution des bulles

Corso L.

Aix-Marseille Université, France (PhD thesis), 2024

Étude quantitative in situ de matériaux réfractaires par diffusion et diffraction des rayons X à haute température

Fowan D.P.

Université de Limoges, Limoges, France (PhD thesis), 2024

Etude de l'impact de l'effet piézoélectrique sur les nanoparticules semi-conductrices à base de nanofils de ZnO pour l'électronique flexible.

Sharma S.

Université Grenoble Alpes, Grenoble, France (PhD thesis), 2024

Study of the interface thermal evolution in bonded SiC substrates for electronics

Le Cunff M.

Université Grenoble Alpes, Grenoble, France (PhD thesis), 2024

Nano-mechanical properties of ZnO piezoelectric semiconductor nanowires

Saidi S.

Aix-Marseille Université, France (PhD thesis), 2024

Highlights ESRF 2024

Operando X-ray diffraction unveils a common degradation path for battery electrode materials,

T. Jousseaume et al., corresponding to ACS Energy Lett. 8, 3323-3329 (2023)https://doi.org/10.1021/acsenergylett.3c00815

1. Actions de formation

En 2025, comme l'année dernière, la ligne a accueilli des groupes d'étudiants en Master 2 et Hercules pour des travaux pratiques sur INS2 et LaueMAX (3 jours). Nous avons réalisé des tutorials au users meeting de l'ESRF (3H) et à l'école européenne HERCULES (2x 4H).